R-curve approach to describe the fracture resistance of tool steels

Ingrid Picas[a], Daniel Casellas[a], Luis Llanes[b]

[a]Fundació CTM Centre Tecnològic, Plaça de la Ciència 2, 08243 Manresa, Spain

[b] CIEFMA - Departament de Ciència dels Materials i Enginyeria Metal·lúrgica, Universitat Politècnica de Catalunya, ETSEIB, Av. Diagonal 647, 08028 Barcelona, Spain

Corresponding author: Daniel Casellas

Tel. +34 93 877 7373

Fax +34 93 877 7374

E-mail address: daniel.casellas@ctm.com.es

ABSTRACT

This work addresses the events involved in the fracture of tool steels, aiming to understand the effect of primary carbides, inclusions and the metallic matrix on their effective fracture toughness and strength. Microstructurally different steels were investigated. It is found that cracks nucleate on carbides or inclusions at stress values lower than the fracture resistance. It is experimentally evidenced that such cracks exhibit an increasing growth resistance as they progressively extend, i.e. R-curve behaviour. Ingot cast steels present a rising R-curve, which implies that the effective toughness developed by small cracks is lower than that determined with long artificial cracks. On the other hand, cracks grow steadily in the powder metallurgy tool steel, yielding as a result a flat R-curve. Accordingly, effective toughness for this material is mostly independent of the crack size. Thus, differences in fracture toughness values measured by using short and long cracks must be considered when assessing fracture resistance of tool steels, especially when tool performance is controlled by short cracks. Hence, material selection for tools or development of new steel grades should take into consideration R-curve concepts, in order to avoid unexpected tool failures or to optimise microstructural design of tool steels, respectively.

1. Introduction

Tool steels for cold forming and shearing applications are typically processed to develop microstructures with large volume fractions of primary carbides embedded in a tempered martensite matrix. They are produced by either ingot cast or powder metallurgy routes followed by hot working, and such microstructure is attained after heat treatment. Alloy carbides are produced by solidification and coexist with austenite during hot working and austenitising. Hot working breaks up the segregated solidification structure. However, alloy carbides are stable during this processing stage; thus, they are elongated and dispersed in bands oriented along with the forging direction. The slow cooling of the conventional static cast ingot drives formation of coarse eutectic carbide structures. As these are difficult to break down during hot working, non-uniform microstructures with marked anisotropy are the final result of the ingot cast metallurgy route (IM). Contrarily, powder metallurgy (PM) tool steels show fine and uniform distribution of carbides as a consequence of rapid solidification during atomisation. Hence, manufacturing process dictates important aspects of the microstructure of tool steels, which in turn controls their mechanical properties and tool performance characteristics.

Microstructural effects on fracture, fatigue and wear behaviour in tool steels have been extensively addressed in the literature during the last three decades [1-12]. The role of carbide size, volume fraction and carbide distribution on fracture properties of tool steel was first studied by Horton and Child [1]. They show that primary carbide nucleates the initial crack and that distribution of carbide clusters affects the crack path through metallic matrix areas, besides determining the quantity of plastic work expended in fracturing the metallic matrix. According to these findings, the fairly superior fracture toughness observed in ingot cast tool steels compared to PM steels was explained by the relatively smaller mean free path between carbides in the latter Owing to the smaller ligament sizes in PM steels, microcracks formed at or in carbides link up with a minimum of plastic deformation of the matrix. [1]. Aimed to understand the different fracture events in tool steels, numerous efforts have been made to determine the stress field in the tempered martensite matrix at the neighbouring of alloy carbides, and to determine the causes for crack nucleation and growth [2-5]. Fracture in tool steels was described by Berns et al. in terms of sequential events: breakage of single alloy carbides due to cleavage leads to a redistribution of stresses which, in turn, causes neighbouring carbides to fracture [2]. Afterwards, bands of plastic deformation in the matrix develop, connecting individual microcracks in carbides. Along these bands, damage takes place in the matrix. Hence, the matrix network acts as an effective obstacle for microcrack linkage. Antretter et al. stated that the shape (which depends largely on the degree of deformation the material has received in the forging process), arrangement and the interaction of each carbide with the local stress field are crucial for determining its breakage [3]. Rammerstorfer et al. showed that the tempered martensite matrix in carbide-rich zones yields at much smaller macroscopic stress levels than in carbide-poor zones; and consequently, cleavage of carbides in such carbide-rich zones occurs at lower applied macro stresses [5]. Bolton and Gant explained the fracture process of tool steels as the formation of voids by carbide cracking, followed by the linking of these voids through deformation of the metallic matrix [6]. Gomes et al. demonstrated experimentally that microcracks initiated in primary carbides grow easily within the carbide band, but they are arrested temporarily (until a higher stress is applied) when reaching the relatively carbide-free region between bands [7].

Tool steels present very high yield stress (usually higher than 2500 MPa) with low elongation at fracture. According to their macroscopic mechanical response as well as usual fracture micromechanisms, they may not be considered as ductile-like materials. Indeed, all previous works dealing with fatigue and fracture resistance of these materials have been analyzed within the framework of linear elastic fracture mechanics [7-12]. Reported values for the fracture toughness measured under plane strain conditions (K_{Ic}) range from 12 to 35 MPa $m^{1/2}$, depending on processing route and resulting hardness (after tempering) of the tool steel. The improvement of the fracture resistance has been continuously stimulated by the industrial needs for high performance tool steels. Manufacture of high strength steel sheets in the automotive sector is a recent and sound example of such statement [13]. Within this context, it is evident that knowledge generated to understand the interaction between cracking phenomena and microstructure in tool steels is highly valuable to improve tool lifetime.

Size, shape and arrangement (within the metallic matrix) of carbides have been identified as key parameters for defining the effective fracture toughness of tool steels. In this regard, a strong interaction arises between microstructurally small cracks and the length of matrix ligaments, pointing out a possible dependency of fracture toughness on crack size for these materials. This usually translates into a rising growth resistance as the crack extends, i.e. *R-curve* behaviour, as it has been extensively reported in many engineering materials, including ceramics [14-17], hardmetals [18,19], metal-matrix composites [20,21], and even bone [22]. Under these conditions, small cracks exhibit stable propagation under applied stress intensity factor values (K) lower than the K_{Ic}, the latter usually assessed on artificially generated long-cracks.

Gomes et al. are amongst the few authors in the open literature dealing with subcritical crack growth in tool steels [4]. They have shown that under increasing monotonic loading, nucleation and growth of natural cracks takes place in these materials at stresses below those for yielding or fracture. In their study, it is postulated that microstructural parameters, rather than macroscopic material properties (which hold for long artificial cracks in the same materials), govern the growth of short cracks. These arguments allow then recalling *R*-curve phenomenon in tool steels.

Notions of *R*-curve are based on the fact that unstable crack propagation requires two conditions to be satisfied: (1) $K \geq K_R$, where K_R is the equivalent stress intensity factor for unstable crack growth; and (2) $dK/da \geq dR/da$, where *dR/da* is the rate of change in material's resistance associated with crack extension (**Fig. 1**). It is interesting to note that such conditions imply that tangency between *K* and *R* depends on the initial crack size (a_0), as shown in **Fig. 1**. As a direct consequence, cracks of distinct sizes may exhibit different effective fracture toughness values.

In IM steels, cracks nucleate in carbides and propagate within a carbide band towards the tougher metallic matrix. The markedly different crack growth resistance between the two phases may result in relevant subcritical crack growth before unstable failure, i.e. crack extension at $K < K_{Ic}$. For a material exhibiting a flat *R*-curve, a single-value toughness unambiguously characterises it, as there is not any stable crack extension, i.e. initial crack size (a_0) is the same as the critical one (a_c). On the other hand, development of a rising *R*-curve implies that toughness is not a single value, as it becomes dependent on stable crack extension. Under these conditions, effective fracture toughness depends on the tangency condition, variable as a function of a_0. In these materials, assessment of *R-curve* behaviour is needed to determine fracture strength, since stable crack growth occurs and the critical crack size is larger than the initial one [14-22].

According to Gomes et al. [7], microcracks initiated in carbides grow easily within bands, but become temporarily arrested (until a higher stress is applied) when reaching relatively carbide-free regions between bands. Likely, these microcracks are initially subcritical-sized flaws that progressively develop into larger cracks, until these eventually satisfy the critical stress intensity condition needed for unstable propagation. In such study, it is shown that non-propagating microcracks are extremely shallow, with a depth not exceeding about 5 µm. However, it completely contrasts with the approximately semi-circular geometry of the observed failure sites. As a consequence, R-curve measurement on the basis of fracture mechanics should include the potential influence of variable crack geometry, from shallow into semi-circular microcracks. Moreover, the intermittent growth/arrest behaviour observed for microcracks would point out that their extension may be extremely dependent on the local microstructure where they are embedded.

Following the above ideas, it is the objective of this investigation to study and analyse initiation and growth phenomena of small cracks, including their corresponding *R*-curve behaviour, for four microstructurally different tool steels. In doing so, macro- as well as micro-mechanical properties are determined by means of fracture tests. Furthermore, local microstructure effects, as related to effective crack geometry as a function of its size, are considered.

2. Experimental procedure

Four different cold work tool steels have been studied in this work. Their chemical composition and processing route are shown in **Table 1**. Primary carbides were identified by means of Field Emission Scanning Electron Microscopy (FE-SEM). The chemical composition of the primary carbides was determined using Energy Dispersive X-Ray Spectroscopy (EDX), with a maximum spot size of about 1 µm, an acquisition time of 10 s and a beam voltage of 10 kV. These parameters were set to ensure small removal of material during detection period; and thus, good accuracy in contents of lightweight elements such as carbon. Crystallographic structure was obtained from the atomic percentage measured in the chemical analysis and comparison with thermo-mechanical calculations obtained by FactSage® software. Carbide amount was quantified through image analysis.

Fracture strength (σ^F) for each studied material was evaluated by means of three-point bending tests, using a constant span length of 40 mm. Prismatic specimens of 5 mm x 4 mm x 50 mm were extracted from forged and annealed commercial bars with their major axis oriented perpendicular (D1), parallel (D2) and transverse (D3) to the forging direction (Fig. 2(a)). Forging results in the elongation and dispersion of the primary carbides forming bands aligned in the same direction; thus, each type of specimen configuration showed different carbide orientation, as schematised in Fig. 2(a). They were mechanically ground and edges were rounded to avoid any stress magnification. Specimens were heat treated aiming to hardness levels about 60 – 62 HRC, which are the most used condition in forming tools (**Table 2**). Surfaces to be subjected to tensile stress during subsequent three-point bending tests were carefully polished to mirror-like finish, using colloidal silica particles. σ^F was evaluated using a universal testing machine, employing an articulated fixture to minimize torsion effects, under applied load rate of 100 N/s. For each tool steel 15 specimens were tested to account for the scatter in the fracture results associated with these materials. Fracture surfaces were examined by means of FE-SEM.

Plane strain mode I fracture toughness (K_{Ic}) was determined in specimens with major axis oriented parallel to the forging direction (specimens D2 in Fig. 2(a)) according to the standard test method ASTM E 399-90 [23]. Large cracks (about 4-5 mm) were propagated from a notch in a single-edge notch bend specimen of 15 x 7.5 x 80 mm using a fatigue resonance machine. Afterwards, cracked specimens were broken under three-point bending to calculate K_{Ic}.

Stress levels for crack nucleation at carbides and subsequent stable growth were evaluated using the same testing set-up and type of specimens described for determining σ^F. Stepwise loading was conducted by increments corresponding to 10 to 15 % fractions of σ^F, as schematised in **Fig. 2(b)** in specimens with orientation D2. Application of each loading step was followed by exhaustive microscopic examination on the specimen face subjected to tensile stresses, by using Light Optical, Confocal Microscopy (CM) and FE-SEM. Such surface observations were conducted aimed to discern damage and corresponding crack-microstructure interaction, in terms of fracture of primary carbides, early growth of cracks, and coalescence of these through the matrix. The tests allow to determine the stress level at which primary carbides start to break. When the first broken carbide is detected, the local stress acting on the carbide can be calculated by considering the distance from the maximum load point at the surface. This stress level is assumed to correspond to the fracture strength of alloy carbides, and it is here referred to as σ^{FC}.

R-curve was constructed from the assessed subcritical crack growth during these stepwise loading tests. Length of cracks at the surface, $2c$, was measured after each applied stress (σ_a). Applied K (K_a) for each crack configuration was then estimated through the equation:

$$K_a = Y \sigma_a \sqrt{a} \qquad \text{(Eq. 1)}$$

As crack depth (beneath the surface), a, measurement was not possible during the tests, K_a was estimated assuming different a/c ratios: 0.3, 0.5 and 1, corresponding to shallow, elliptical and semi-circular shaped cracks. Y values were calculated on the basis of equations given by Newman and Raju [24]. In order to determine experimentally the real shape of small surface cracks, sequential polishing was performed in specimens of one investigated tool steel (UNIVERSAL), tested at stress levels close to fracture strength but halted some instants before failure. Changes in size of a dummy Rockwell C imprint, introduced close to the studied cracks, were used for precise control of the amount of material removed during polishing; and thus, direct measurement of crack depth. FE-SEM inspections were performed after each step to register changes in crack morphology.

3. Experimental results

3.1 Microstructure, flexural strength and fracture toughness

The microstructure of the studied steels is showed in **Fig. 3**. Steel referred to as 1.2379 exhibits a markedly anisotropic microstructure (**Fig. 3a**), with large carbides forming bands. This is also the case for K360 material (**Fig. 3c**), although a more homogeneous carbide distribution is discerned for this steel. Microstructural heterogeneity is even less pronounced for UNIVERSAL steel (**Fig. 3e**), but preferential carbide alignment following the forging direction is still observed. Finally, HWS material presents a typical PM tool steel isotropic microstructure (**Fig. 3g**), with very small spherical carbides uniformly distributed in the metallic matrix. Chemical composition and amount of primary alloy carbides are listed in **Table 3**. One type of primary carbide, M_7C_3- (**Fig. 3b**) is exclusively found in 1.2379 steel. On the other hand, three different primary carbides: M_7C_3, MC and M_6C (**Fig. 3d**), are identified in K360 material. An intermediate scenario, M_7C_3 and MC primary carbides, is evidenced in UNIVERSAL and HWS steels (**Figs. 3f and 3h**).

Fig. 4(a) shows the average σ^F of the studied steels. Fracture strength of 1.2379, UNIVERSAL and K360 D2 is significantly higher than D1 and D3, while HWS shows very similar fracture behaviours in all three configurations. These results are in agreement with the microstructures that have been observed in these steels. IM steels are rather anisotropic due to their marked carbide fibre orientation. On the other hand, PM steels are more isotropic, as expected after its very fine and homogeneous carbide distribution. HWS shows the highest σ^F results amongst the studied materials. UNIVERSAL has higher σ^F values than

K360 and 1.2379, and in addition UNIVERSAL D1, D2 and D3 show less difference than K360 and 1.2379 D1, D2 and D3. In turn, 1.2379 has the lowest and the most anisotropic fracture results. The values of K_{Ic} obtained in the D2 direction for the steels under consideration are shown in **Table 4**. They are markedly higher for 1.2379, K360 and UNIVERSAL steels than for HWS. These results are in agreement with previous works [1], where higher fracture toughness of IM steels was attributed to the increased length of matrix ligaments, as compared to that found in PM steels.

Fractographic inspection points out that failure initiation sites are primary carbides, or agglomerates of them, in IM steels (**Fig. 5a**). On the other hand, inclusion particles are identified to be critical failure locations in HWS material, as it is commonly the case for PM steels. Fracture usually starts from approximately semi-circular “thumbnail” regions, sometimes clearly identified by the “river markings” radiating from them (**Fig. 5b**). As it is shown in **Figure 5c**, the final length of cracks discerned at the surface is delimitated by high plastically deformed zones at the fracture edge.

3.2 Fracture of primary carbides: effective crack nucleation strength

Breakage of carbides is related with dislocations pin up and cleavage of the matrix at carbide/matrix interfaces, prior to attain σ^F. Hence, a critical applied stress driving carbides to fail can be determined and related to the onset for crack nucleation in carbides for each tool steel microstructure. This stress level has been experimentally measured in the incremental stepwise bending tests, and it is here referred to as σ^{FC}. Such small-scale failure stress depends not only on the carbide intrinsic properties (as fracture toughness, property measured by nanoindentation in a previous work [25]), but also on microstructural features such as carbide shape and/or carbide band characteristics, since they locally raise the macroscopically applied stress and induce carbide fracture [5]. As a result, σ^{FC} values can vary substantially from steel to steel depending on nature, shape, size and arrangement of alloy carbides. The values of σ^{FC} of the different carbides present in the studied steels, determined following the stepwise loading method showed in Fig. 2(b), are plotted in Fig. 4(b) together with the σ^{F} for each steel. It clearly shows for every carbide that σ^{FC} is always lower than σ^{F}.

From Fig. 6, σ^{FC} of M_7C_3 carbides for 1.2379 steel is estimated to be about 800 MPa. Limited data are available in the literature to contrast this result. In this regard, a stress value of about 1100 MPa for carbide rupture in SKD11 steel was reported by Fukaura et al. [26]. Although 1.2379 and SKD11 are equivalent steels in terms of chemical composition, applied heat treatments and forging processes may have been different; thus, final shape, size and distribution of primary carbides could also be quite distinct in both studies. Taking this into consideration, relative agreement between σ^{FC} values measured for 1.2379 and SKD11 steels may then be described as satisfactory.

σ^{FC} values for M_7C_3 and MC carbides in K360 steel are estimated to be about 600 MPa and 1400 MPa respectively. The shape of M_7C_3 carbides in this steel is rather irregular, and their size is slightly higher than that of similar carbides in 1.2379 material. On the other hand, MC carbides are rounder (more regular) than M_7C_3 ones, these being main reasons for the higher σ^{FC} exhibited by the former as compared to the latter. Similarly, σ^{FC} value for M_7C_3 carbides in UNIVERSAL is higher (about 1400 MPa) than in 1.2379 and K360 steels, owing to their smaller and rounder shapes. MC carbides of UNIVERSAL are even smaller and more regular than the M_7C_3 ones. As a result, they have the highest σ^{FC} value amongst the studied ingot steels (around 1700 MPa). Such a trend gets to the limits for the PM tool steel HWS. Here, carbides exhibit σ^{FC} values close to those determined as σ^{F} for the steel itself.

Fig. 6 presents some representative examples of carbides and inclusions broken in the studied steels. Once cracks are nucleated in carbides (in IM steels) or inclusions (PM steels), a plastic zone in the matrix is developed ahead of the crack tip (**Figs. 7a** and **7b** for IM and PM steels respectively). Microcrack formation in the matrix takes place within such high plastically deformed regions. These cracks grow and coalesce with each other, leading to a main propagating crack that causes final failure of the specimen (as it is neatly shown in the sequence of images of **Fig. 8**). However, the stable crack growth regime in HWS is very short, and experimental recording of subcritical crack propagation is extremely hard for this material. Opposite to IM steels, cracks nucleate at very high stresses in HWS steel; thus, transition period between nucleation and unstable fracture is indeed extremely short (**Fig. 9**).

3.3. Growth and coalescence of cracks: interaction with microstructure

Experimental results show that crack nucleation and growth in IM steels takes place at stresses below those for fracture under increasing monotonic stresses. Within the framework of short cracks, knowledge about flaw geometry is then required in order to determine accurately applied *K* values (K_a). However, crack geometry is usually unknown, since they run inwards from the surface specimen. Aiming to overcome these uncertainties on the real geometry of cracks, sequential polishing was used to determine the depth of different cracks observed at the surface (**Fig. 10**). **Fig 10d** shows the experimentally measured *a/c* ratio for each of the studied cracks. Results shows that crack depth profiles are tortuous; thus, crack depth is rather variable. In this study, *a* values are calculated as the minor axis of the equivalent semi-ellipse which fits the corresponding crack depth profile.

Following the above results, and in agreement with the findings reported by Gomes et al. [7], non propagating cracks (i.e. those still within the limits of the carbide band) are initially shallow, e.g. cracks 2 and 4 in **Fig. 10**. On the other hand, propagating cracks (i.e. those crossing the matrix band) tend to evolve to semicircular configuration before fracture, e.g. cracks number 1 and 3 in **Fig. 10**. The shape of the crack (*a/c* ratio) determines the *K* values at 0º and 90º from the surface. The stress intensity factor for shallow cracks ($a/c < 1$) yields K^{90} values higher than K^{0} ones [24]. It means that shallow cracks grow preferentially perpendicular to the surface. As a consequence, *a* value increases faster than the *c* one. As the ratio *a/c* approaches 1, K^{90} and K^{0}

values become similar, and so is the crack growth in both perpendicular and parallel directions to the surface.

The final geometry of the cracks is strongly influenced by the local microstructure ahead of the crack tip. Reasons for some cracks running deeper and faster than others can be related to either size of the carbide band in which they are initially embedded and/or the probability of finding the next carbide band. Indeed, these ideas also explain the rapid development of semicircular shape cracks in HWS, since no microstructural discontinuities are present in front of cracks for this tool steel.

R-curve behaviour for the studied tool steels has been assessed by measuring the increase of crack length at the surface ($\Delta 2c$) resulting for each step-incremental applied stress (σ_a), and estimating the corresponding K_a. Results are summarised in **Fig. 11**. As the real geometry of cracks gradually evolves from very shallow ($a/c < 1$) into semi-circular ($a/c = 1$) shapes, three possible *R*-curves have been constructed for each material, considering a/c values of 0.3, 0.5 and 1. The mathematical description proposed by Evans (**Eq. 2**) may describe with good accuracy the *R*-curve behaviour of structural materials [27]:

$K_a = K_0 + C_1 \cdot atan\ (\Delta a/C_2)$ (Eq. 2) where K_0, C_1 and C_2 are constants relating K_a and Δa. According to the plots of K_a vs $\Delta 2c$ (**Fig. 11**), Eq. 2 can be rewritten in terms of $\Delta 2c$ (assuming a/c = 0.3, 0.5 or 1). Best-fit K_0, C_1 and C_2 values are shown in **Table 5**.

It can be observed that although *R*-curves estimated assuming different a/c values tend to converge to the same K_a at high $\Delta 2c$ values, at low $\Delta 2c$ values shallow cracks (a/c = 0.3 and 0.5) exhibit lower K_a values than semi-circular cracks (a/c = 1). Semi-circular cracks attain the toughness plateau value at lower crack extensions than shallow ones. It may then be stated that K_a values for semi-circular cracks have less dependency upon crack size than in shallow ones.

Regardless of the a/c ratio, 1.2379 steel shows a more pronounced *R*-curve behaviour; i.e. plateau value is attained at larger $\Delta 2c$ values, than K360 or UNIVERSAL materials. On the other hand, HWS steel shows a quite steep-rising *R*-curve, i.e. plateau value is reached after extremely short stable crack propagation. Cracks analysed for 1.2379 and K360 steels do not attain K_{Ic} at the measured plateau in the *R*-curve. On the other hand, *R*-curve plateau coincides with K_{Ic} value experimentally measured for UNIVERSAL and HWS materials. It means that even for the longest cracks considered in *R*-curve plots, the effective toughness before failure (or K_R) for 1.2379 and K360 steels is lower than the potential K_{Ic} that those materials could develop.

As described in section 1, the *R*-curve behaviour implies that *K* values for unstable fracture (K_R) may vary depending upon initial crack size. Thus, it should be estimated as the K_a value tangent to the *R*-curve, for different $2c_0$ values, as schematised in **Fig. 1**. It may be done from *R-curves* presented in **Fig. 11**, by considering tangency condition for different initial crack lengths ($2c_0$) and $a/c = 1$ ($a/c < 1$ has not been considered, since final crack geometries tend to approach $a/c \approx 1$). **Fig 12a** shows, as an example, the procedure followed for calculating K_R corresponding to different $2c_0$ values. Overall K_R results are plotted in **Fig. 12b**.

4. Discussion

In the studied tool steels, it has been experimentally evidenced that as applied stress increases, cracks are nucleated at primary carbides or inclusion particles, and subsequently grow through the metallic matrix. Carbides and matrix exhibit an excellent adhesion; thus, cracks easily cross through the interface. However, due to the lower toughness of the primary carbides (in the range of 2-4 $MPa \cdot m^{1/2}$, as measured by nanoindentation [25]), as compared to the metallic matrix (evaluated as about 38 $MPa \cdot m^{1/2}$ for 1.2379 tool steels [28]), the nucleated cracks do not grow immediately. An increase of the external stress is required to meet the propagation criterion, i.e. K_a higher than the initial crack growth resistance. In this work, it has been postulated and validated that crack propagation requires a successive increase of the applied stress, since the material resistance to fracture rises as the crack grows. Such a response is known as *R*-curve behaviour and leads to important design considerations, since effective toughness of short and large cracks can be quite different. IM steels, especially 1.2379 and K360, show a pronounced *R-curve.* On the other hand, PM steels (such as HWS material) show a steep-rising *R-curve,* with very low dependency of K_R on the initial crack size.

The development of *R-curve* behaviour in tool steels may be rationalised by the progressive development of a plastic zone in front of the crack tip as it grows. As it is shown in **Fig. 8**, any crack propagation under monotonic loading is preceded by plastic deformation of the metallic matrix around broken primary carbides. Cracks are initially very shallow, but they gradually develop into semi-circular shapes as they propagate in a stable manner. Although many cracks nucleate and start propagating at the specimen surface, only very few of those attain long sizes, and corresponding *a/c* ratios close to 1. Plastic deformation at the crack tip progressively increases with applied stress until the matrix finally breaks, triggering then crack growth. Then, cracks are again arrested until stress is increased, and more plastic deformation is induced around the newly generated crack tip. Cracks grow further and tend to coalesce with each other, until they finally lead to specimen failure. The measured size of the plastic zone (r_p) in the tested specimens is very small (about 5 to 10 μm) compared to the crack size before fracture (100-200 μm). These values are similar to the theoretical ones calculated assuming plain stress conditions:

$$r_P = \frac{1}{2\pi} \cdot \frac{K_I^2}{\sigma_Y^2} \qquad \text{(Eq. 3)}$$

where σ_y is the yield stress of the material (in the studied materials σ_y is about 90% of the σ^F). Such small plastic zones shows the limited plasticity of tool steel, and sustain the use of linear elastic fracture mechanics concepts to describe their fracture resistance, as it has been reported by many authors previously [7-12]. As shows Eq. 3, the size of the plastic zone in the matrix ahead of a crack tip is related to the applied K, but it also depends on the available volume of metallic material that can sustain plasticity. Tool steel microstructures consist of a dispersion of carbides in a tempered martensite matrix, the main toughening mechanism being the plastic deformation of such matrix. Thus, to attain the full plastic deformation potential of the tool steel, a large volume of metallic matrix should be affected by the propagating crack.

Above findings are relevant to understand subcritical growth of microcracks in tool steels and assess potential *R*-curve behaviour. IM steels show a clear dependency of toughness on crack size, i.e. a rising *R*-curve, whose characteristics are intimately related to the specific steel microstructure. Accordingly, toughness is size dependent in IM steels, i.e. effective fracture toughness may differ (always in the lower side) from the toughness value assessed by using long artificial cracks, i.e. K_{Ic}. On the other hand, the evaluated PM steel is found to exhibit a steep-rising *R*-curve; therefore, toughness results to be independent of the initial crack size. One relevant consequence of this rising R-curve behaviour is that maximum toughness level that natural cracks (size up to 200 μm in the fracture tests) may attain is quite similar to that evaluated with large cracks (in the range of 3-5 mm) following the ASTM standard.

The highest K_R that may be developed at the measured R-curves, i.e. the plateau level of the rising R-curve, is named $K_{R,MAX}$. It is listed in **Table 5**, and compared with K_{Ic} values. The difference between $K_{R,MAX}$ and K_{Ic} is specially relevant for 1.2379 and K360 steels (as it is clearly seen in **Fig. 11**). Such results are in agreement with those reported by Gomes et al., where $K_{R,MAX}$ in the range 0.5-1K_{Ic} were found for high speed steels [7] .

An interesting mechanical design implication of *R-curve* behaviour is related to the correlation of the toughness level with the fracture strength. In order to better understand the relation between fracture toughness, crack size and failure stress, K_R is plotted against the fracture strength, σ^F, for different crack sizes in **Fig 13a**. It is found that both parameters follow a linear inverse relationship in the crack size range from 20 to 2000 μm. A material without any R-curve behaviour (i.e. flat *R*-curve) would not show any toughness-strength dependence, since K_R does not vary with the crack size and is equal to K_{Ic}. On the other hand, the more pronounced the corresponding R-curve behaviour (more negative slopes), the larger the differences between K_R for small and large cracks.

The experimentally assessed *R-curve* behaviour has also important design considerations from the viewpoint of its application as forming tool. In this regard, if the effective toughness depends on the crack size, the tool steel performance would also change for different forming processes depending on the stress level acting on tools. Main reason behind it is the fact that critical flaw size for failure finally depends on the applied stress. One of the prominent fracture mechanisms in forming tools is fatigue [29, 30]. At high stress levels, crack size at fracture will be rather short. According to the experimental findings of this investigation, the toughness level developed by the R-curve will then be lower than expected from ASTM tests with long cracks. Within this context, 1.2379 and K360 steels would not ever reach K_{Ic} level (**Table 4**). It means that whether small cracks or high loads are involved in the fracture process, both steels will show fracture instability at significantly lower toughness levels than those expected from K_{Ic} ones. Very interesting, the UNIVERSAL tool steel shows not only the highest K_{Ic} value but also outstanding potential of short cracks to reach K_{Ic} value (note that $K_{R,max}$ and K_{Ic} are quite close to each other, **Table 4**). Thus, UNIVERSAL tool steel may be defined as the closest to ideal behaviour amongst the IM steels considered. On the other hand, HWS material exhibits a practically flat *R*-curve. It means that small cracks in HWS will not show any toughness dependence on crack size. However, K_{Ic} for this steel is still low compared to the effective toughness values assessed for the ingot steels.

The *R-curve* behaviour of tool steels has important implications to understand fracture performance of industrial tools, since the fracture strength calculated from K_{Ic} using fracture mechanics concepts (Eq. 1) can substantially differ from the effective one attained under real service conditions. As an example, in tools for shearing ultra high-strength steels sheets, stresses of about 1500 MPa and even higher are developed in tools, as it has been estimated by Picas et al. [31] and Nothhaft et al. [32]. In **Figure 14a** and **Table 4**, it is shown the effective K_R value developed by the different tool steels. For 1.2379 and K360 materials, the relative difference between K_{Ic} and the estimated K_R at 1500 MPa is about 30%. Meanwhile, it is only 7% and 3% in UNIVERSAL and HWS steels, respectively. As it follows from these results, in tools made of IM steels the reduction of effective toughness associated with small cracks, as compared to the K_{Ic} values, may become extremely significant. As a final result, K_R values for IM steels could be similar or even lower than those for PM steels. It could then give rise to unexpected in-service behaviour, where tool steels with lower K_{Ic}, as PM tool steels in front of IM ones, show better mechanical performance in terms of toughness. Within this context, it is plausible to say that in tools subjected to high stresses, as those for shearing ultra high-strength steel sheets, a PM-type microstructure (e.g. HWS tool steel), could offer not only higher resistance to crack nucleation (breakage of primary carbides) but also higher effective toughness (K_R) than IM steels, as far as small cracks are nucleated in the microstructure. As it follows from **Fig. 14**, for cracks smaller than 500 µm, PM steels (HWS steel) may effectively exhibit higher K_R values than some IM ones (1.2379 and K360 steels). On the other hand, if the applied stresses are relatively low, so that nucleated cracks can grow to longer sizes (more than 500 µm), an IM steel type microstructure will then show a better performance than HWS, since K_R for the former would be higher than for the latter.

5. Conclusions

In this work the fracture resistance of different tool steels is described through a *R-curve* approach. From the experimental evaluation of the microstructural features and the crack growth mechanisms the following conclusions can be drawn:

(1) The nucleation of cracks in tool steels is due to the failure of primary carbides by cleavage (and inclusion particles in case of PM steels) when the stress exceeds their fracture strength, σ^{FC}. Primary carbides in 1.2379 and K360 present the lowest σ^{FC} results, while those in UNIVERSAL show higher values of σ^{FC}. HWS, in turn, shows the highest σ^{FC} results. This means that HWS has very high resistance to crack nucleation at primary carbides or inclusions compared to IM steels.

(2) Small cracks nucleated from primary carbides in IM steels are initially very shallow, but they tend to grow to semi-circular shapes as the load increases and they propagate through the matrix bands. In HWS, small cracks are semi-circular from the early propagation stage and they grow steadily through the microstructure.

(3) Fracture resistance of tool steels can be described by an R-curve approach: cracks nucleated in carbides or inclusions propagate through the microstructure and the attained toughness depends on the initial crack size. IM steels show a

continuous rising R-curve, which means that toughness depends on crack growth. The initial slope of the R-curve depends on the tool steel microstructure, being it higher in the UNIVERSAL steel than in 1.2379 and K360 ones. The studied powder-metallurgy steel, on the contrary, shows a steep-rising R-curve, with a very low dependence of toughness with respect to the initial crack size.

(4) In some ingot cast tool steels (1.2379 and K360), their pronounced *R*-curve behaviour give rise to marked differences between the toughness developed by small cracks and the one measured using large cracks. The maximum toughness developed by natural cracks is lower than the values of K_{Ic} measured following ASTM E399 procedure. The difference between both toughness levels increases when cracks are small. In the other ingot cast tool steel studied, the UNIVERSAL steel, toughness of small natural cracks and K_{Ic} values are close to each other.

(5) The R-curve behaviour has important considerations for tool performance because in cold forming tools fracture is triggered by small cracks, and then the effective toughness may considerably differ from K_{Ic}. It is especially relevant when tools are subjected to high stress levels, where cracks involved in tool failure are rather short.

(6) For high performance tools, with expected high fracture resistance, the choice of material based on K_{Ic} may lead to inappropriate decisions, yielding then unexpected tool fractures. Ingot cast steels use to show larger K_{Ic} values

than PM ones. However, some ingot cast steels do not reach such K_{Ic} value for short cracks, and their effective toughness can be similar or even lower than for PM steels. Therefore, tool steel selection for a given application should be conducted taking into account the overall R-curve behaviour and the stress level acting on the tool, since fracture resistance of the material may vary substantially.

Acknowledgements

This work has been partially funded by ACC1Ó (Grant TECRD12-1-0012 and TECCTA-13-1-0005) and the Spanish Ministerio de Economía y Competitividad (Grant MAT2012-34602). The authors would like to express their gratitude to Prof. Jean Steinmetz, at Jean Lamour Institute (France) for the in-depth analysis of carbides in K360 tool steel.

References

[1] S.A. Horton and H.C. Child: Met. Technol., 1983, vol. 10, pp. 245-56

[2] H. Berns and C. Broeckmann: Eng. Frac. Mec., 1997, vol. 58, pp. 311-25

[3] T. Antretter and F.D. Fischer: Mater. Sci. Eng. A, 1997, vol. 237A, pp. 6-11

[4] H. Berns, A. Melander, D. Weichert, N. Asnafi, C. Broeckmann and A. Groβ-Weege: Comput. Mater. Sci., 1998, vol. 11, pp. 166-80

[5] F.G. Rammerstorfer, A.F. Plankensteiner, A.D. Fischer and T. Antretter: Mater. Sci. Eng. A, 1999, vol. 259A, pp. 73-84

[6] J.D. Bolton and A.J. Gant: J. Mater. Sci., 1998, vol. 33, pp. 939-53

[7] M.A. Gomes, A.S. Wronski and C.S. Wrigth: Int. J. Fract., 1997, vol. 83, pp. 207-21

[8] S-H. Choo, C. Kyu, K. Euh, S. Lee, J.-Y- Jung and S. Ahn: Metall. Mater. Trans. A, 2000, vol. 31A, pp. 3041-52

[9] F. Meurling, A. Melander, M. Tiedesten and L. Westin: Int. J. Fatigue, 2001, vol. 23, pp. 215-24

[10] K. Shiozawa, L. Lu and S. Ishihara: Fatigue Fract. Engng. Mater. Struct., 2002, vol. 24, pp. 781-90

[11] C.R. Sohar, A. Betzwar-Kotas, C. Gierl, B. Weiss and H. Danninger: Int J. Fatigue, 2008, vol. 30, pp. 1137-49

[12] D. Das, R. Sarkarb, A. K. Duttac and K. K. Rayd: Mat. Sci. Eng. A, 2010, vol. 528A, pp. 589-603

[13] I. Picas I, R. Hernández, D. Casellas, B. Casas, I. Valls, Mechanical performance of cold forming tools, in Proc. 8th Int. Tooling Conf., P. Beiss, C. Broeckman, S. Francke and B. Keysselitz eds., Aachen, Germany; 2009, pp. 1037-48

[14] T. Fett and D.Munz: J. Mater. Sci., 1993, vol. 28, pp. 742–52

[15] D. Casellas, J, Alcalá, L. Llanes and M. Anglada: J. Mat. Sci., 2001, vol. 36, pp. 3011-25

[16] D. Munz: J. Am. Ceram. Soc., 2007, vol. 90, pp. 1–15

[17] J. J. Kruzic, R. L. Satet, M. J. Hoffmann, R. M. Cannon and R. O. Ritchie: J. Am. Ceram. Soc., 2008, vol. 91, pp. 1986–94

[18] P.A. Mataga: Acta Mater., 1989, vol. 37, pp. 3349–59

[19] Y. Torres, R. Bermejo, L. Llanes and M. Anglada: Eng. Frac. Mech., 2008, vol. 75, pp. 4422-30

[20] O. Sbaizeroa, G. Pezzottia and T. Nishidaa: Acta Mater., 1998, vol. 46, pp. 681-7

[21] R.R. Adharapurapu, K.S. Vecchio, F. Jiang and S. Rohatgi: Metall. Mater. Trans. A, 2005, vol. 36A, pp. 3217-36

[22] R.O. Ritchie, K.J. Koester, S. Ionova, W. Yao, N.E. Lane and J.W. Ager III: Bone, 2008, vol. 43, pp. 798-812

[23] ASTM E399-09. Standard test method for linear-elastic plane-strain fracture toughness K_{Ic} of metallic materials. American Society for Testing and Materials. West Conshohocken, PA, USA; 2009

[24] J.C. Newman and I.S. Raju: Eng. Mater. Struct., 1992, vol. 15, pp. 1141-53

[25] D. Casellas, J. Caro, S. Molas, J.M. Prado and I. Valls: Acta Mater., 2007, vol. 55, pp. 4277-86

[26] K. Fukaura, Y. Yokoyama, D. Yokoi, N. Tsuji and K. Ono: Metall. Mater. Trans.A, 2004, vol. 35A, pp. 1289-300

[27] A.G. Evans, Toughening mechanisms in zirconia alloys, in Advances in Ceramics: Science and Technology of Zirconia II, N. Claussen, M. Rühle and A.H. Heuer eds., Am. Ceram. Soc., Columbus OH, (1980) pp. 193-212

[28] P. Muro, S. Gimenez and I. Iturriza: Scripta Mater., 2002, vol. 46, pp. 369-73

[29] M.R. Krishnadev and S.C. Jain: Eng. Fail. Anal., 2007, vol. 14, pp. 1053-64

[30] S.Y. Luo: J. Mater. Process. Technol., 1999, vol. 88, pp. 122-33

[31] I. Picas, R. Hernández, D. Casellas, B. Casas, I. Valls, Tool performance in cutting of hot stamped steel, in Proc. 1st Hot Sheet Metal Forming of High-Performance Steel, K. Steinhoff, M. Oldenburg and B. Prakash eds., Kassel, Germany, 2008, pp. 179-89

[32] K. Nothhaft, J. Suh, M. Golle, I. Picas, D. Casellas and W. Volk: Prod. Eng. Res. Devel., 2012, vol. 6, pp. 413-20

TABLES

Table 1

Chemical composition (in wt %) and processing route (ingot metallurgy, IM, or powder metallurgy, PM) of the studied steels. K360 ISODUR is produced by BÖHLER EDELSTAHL GmbH & CO KG. UNIVERSAL and HWS steels are produced by ROVALMA S.A.

Steel	Process	C	Cr	Mo	V	W	Others
DIN 1.2379	IM	1.5 – 1.6	11.0 – 12.0	0.6 – 0.8	0.9 – 1.0	-	-
K360	IM	1.2 – 1.3	8.0 – 9.0	2.0 – 3.0	1.0 – 1.5	-	+ Nb +Al
UNIVERSAL	IM	0.9 – 1.2	6.8 – 8.5	-	2.5 – 3.0	1.1-1.4	-
HWS	PM	0.9 – 1.2	6.8 – 8.5	-	2.5 – 3.0	1.1-1.4	-

Table 2

Heat treatment applied to the studied materials and obtained hardness level.

Steel	Austenitizing (quench in oil)	Tempering	HRC
1.2379	1050 ºC for 30 min	550 ºC for 2 h (x2)	60 - 62
K360	1060 ºC for 30 min	450 ºC for 2 h (x3)	60 - 62
UNIVERSAL, HWS	1060 ºC for 35 min	540 ºC for 2 h (x3)	60 - 62

Table 3

Structure, amount and chemical composition (in wt %) of the primary alloy carbides.

Tool Steel	Carbide structure	Amount %	V	Cr	Fe	Mo	W	Nb	Ti	Si
1.2379	M_7C_3	11.2 $^{(a)}$	3.5	42.2	44.2	2.1	-	-	-	-
K360	M_7C_3	6.1 $^{(a)}$	6.3	38.5	39.9	6.9	-	-	-	-
K360	MC	0.8 $^{(a)}$	6.5	-	-	-	-	75.4	1.5	-
K360	M_6C	1.0 $^{(a)}$	3.4	6.1	33.7	50.1	-	-	-	3.4
UNI	M_7C_3	2.1 $^{(a)}$	7.7	38.4	40.0	3.3	2.2	-	-	-
UNI	MC	3.8 $^{(a)}$	61.3	10.8	2.0	3.8	4.0	-	-	-
HWS	M_7C_3 $^{(b)}$	3.7	7.7	38.4	40.0	3.3	2.2	-	-	-
HWS	MC $^{(b)}$	4.4	61.3	10.8	2.0	3.8	4.0	-	-	-
HWS	M_6C $^{(c)}$	<0.1	*	*	*	**	**	-	-	-

(a) Amount of carbides with an *ECD* > 5 μm

(b) Chemical composition of carbides is considered to be same as the UNIVERSAL

(c) Structure and chemical composition could not be determined accurately using EDX

Table 4.

K_{Ic} (E 399-90), K_R estimated at 1500 MPa and the difference calculated between these two parameters for a/c = 1.

K, MPa·m$^{1/2}$	1.2379	UNIVERSAL	K360	HWS
K_{Ic} (E 399-90)	28.1	29.4	28.6	21.0
$K_{R,MAX}/K_{Ic}$	0.92	0.99	0.78	1.0
K_R (at 1500 MPa)	20.0	27.7	20.3	20.4
K_R (at 1500 MPa) / K_{Ic}	0.71	0.94	0.70	0.97

Table 5

Best-fit parameters (K_0, C_1 and C_2) in Eq. 3, to describe R-curve behaviour for each of the studied tool steels, and *A* and K_{Rmax} parameters in Eq. 4.

Steel	a/c	K_0, MPa·m$^{1/2}$	C_1, MPa·m$^{1/2}$	C_2, µm	$K_{R,MAX}$ MPa·m$^{1/2}$
1.2379	0.3	2.8 ± 0.6	15.1 ± 0.1	217.7 ± 35.4	-
	0.5	3.2 ± 0.8	15.3 ± 0.6	165.6 ± 32.8	-
	1	4.1 ± 1.3	13.3 ± 1.4	42.4 ± 11.4	26.0
K360	0.3	2.1 ± 0.3	14.7 ± 0.4	106.2 ± 14.3	-
	0.5	2.8 ± 0.2	13.1 ± 0.3	58.2 ± 6.5	-
	1	4.3 ± 0.7	11.6 ± 0.6	23.8 ± 5.9	22.4
UNIVERSAL	0.3	2.9 ± 0.4	17.9 ± 0.5	96.9 ± 9.5	-
	0.5	3.8 ± 0.54	16.8 ± 0.6	51.8 ± 5.4	-
	1	5.0 ± 0.9	16.3 ± 1.0	26.6 ± 3.9	29.3
HWS	0.3	3.2 ± 0.4	12.4 ± 0.5	34.6 ± 8.6	-
	0.5	4.6 ± 0.5	11.1 ± 0.5	17.5 ± 3.3	-
	1	6.4 ± 0.6	9.8 ± 0.6	8.3 ± 1.5	21.0

Figure Captions

Fig. 1. Crack growth resistance behavior: failure instability condition occurs in the cracked solid when *dK/da = dR/da.*

Fig. 2. (a) Orientation of tested specimens with respect to the forging direction; perpendicular (D1), parallel (D2) and transverse (D3). **(b)** Description of stepwise monotonic tests and surface inspections. The inspected zone in the face subject to tensile stresses of the samples is shown.

Fig. 3. FE-SEM images showing microstructure of the studied tool steels: (a)-(b) 1.2379, (c)-(d) K360, (e)-(f) UNIVERSAL, and (g)-(h) HWS.

Fig. 4. (a) Fracture strength of the studied tool steels (σ^F) with different orientations related to the rolling direction (D1, D2, D3) (b) Fracture strength of primary carbides (σ^{FC}), compared to the σ^F for each steel (orientation D2).

Fig. 5. Failure initiation site in K360 obtained by FE-SEM. (a) Initial cracked carbide. (b) “River markings” emanating from the initial cracked carbide and semi-circular “thumbnail” region. (c) Crack length at the surface delimited by high plastically deformed zones at the fractured edge.

Fig. 6. Broken particles at corresponding σ^{FC} level: (a) M_7C_3 in 1.2379, (b) M_7C_3 in K360, (c) MC in K360, (d) M_7C_3 in UNIVERSAL, (e) MC in UNIVERSAL, (f) non-metallic inclusion in HWS, and (g) carbides in HWS.

Fig. 7. Plastic bands developed in the matrix ahead of the tip in (a) cracked carbides, and (b) inclusion particles.

Fig. 8. Crack growth evolution at the surface of a K360 sample with increasing applied stress: (a) 1600 MPa, (b) 1900 MPa, (c) 2200 MPa, and (d) 2600 MPa. (e) Fracture at 2964 MPa. Images from (a) to (d) are obtained by CM and different colours are indicative of the surface topography: bluish mean sunk/deformed zones and reddish uplifted zones. Image (e) Is obtained by FE-SEM, and is rotated 90º with respect to the previous ones.

Fig. 9. Crack growth evolution at the surface of a HWS sample with increasing applied stress. (a) 3500 MPa, (b) 3800 MPa, (c) 4200 MPa. (d) Fracture at 4370 MPa. Images are obtained by CM and different colours are indicative of the surface topography: bluish mean sunk/deformed zones and reddish uplifted zones.

Fig. 10. Cracks observed at the surface of the UNIVERSAL sample tested under monotonic loading and stopped before failure: (a) crack number 1: 2c ≈ 192 μm, (b) cracks number 2 and 3: 2c ≈ 124 μm and 154 μm respectively, and

(c) crack number 4: 2c ≈ 103 μm. (d) Crack depth profile and a/c value for cracks labelled 1, 2, 3 and 4 (a is the crack depth and *2c* is the crack length)

Fig. 11. *R*-curves considering different *a/c* ratios (0.3, 0.5 and 1): (a) 1.2379, (b) K360, (c) UNIVERSAL, and (d) HWS materials.

Fig. 12. (a) Unstable fracture condition as a function of initial crack length, $2c_0$, and *a/c* = 1, for DIN 1.2379, (b) Calculated K_R values following the procedure shown in Fig 12(a) at different $2c_0$.

Fig. 13. Applied stress intensity factor for unstable fracture (K_R) vs the corresponding applied stress (σ_a) considering different $2c_0$ values and *a/c* = 1. Vertical line indicates a stress level of 1500 MPa that can be developed in cold forming tools

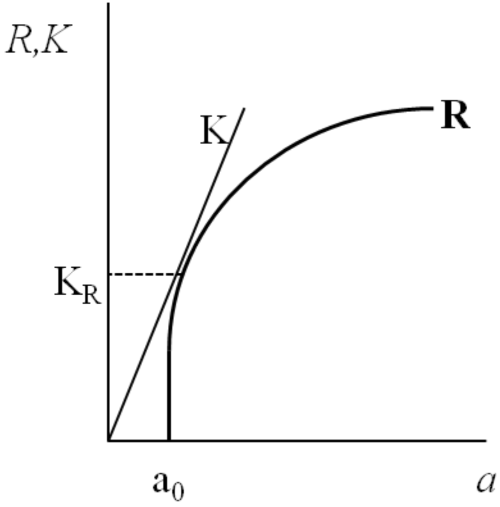
R,K
K
R
K_R
a_0
a

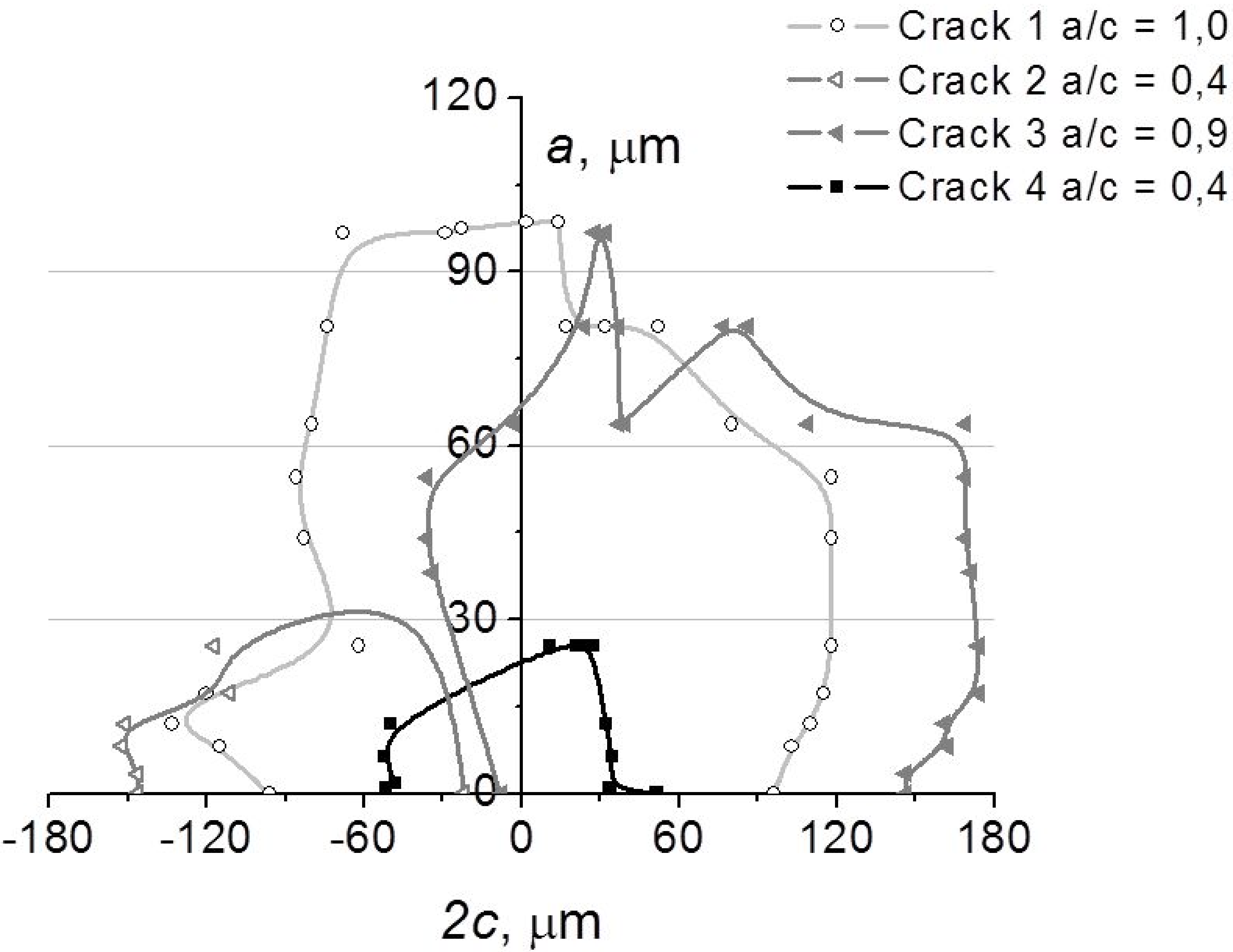
Crack 1 a/c = 1,0
Crack 2 a/c = 0,4
Crack 3 a/c = 0,9
Crack 4 a/c = 0,4
120
90
60
30
0
a, μm
-180
-120
-60
0
60
120
180
2*c*, μm

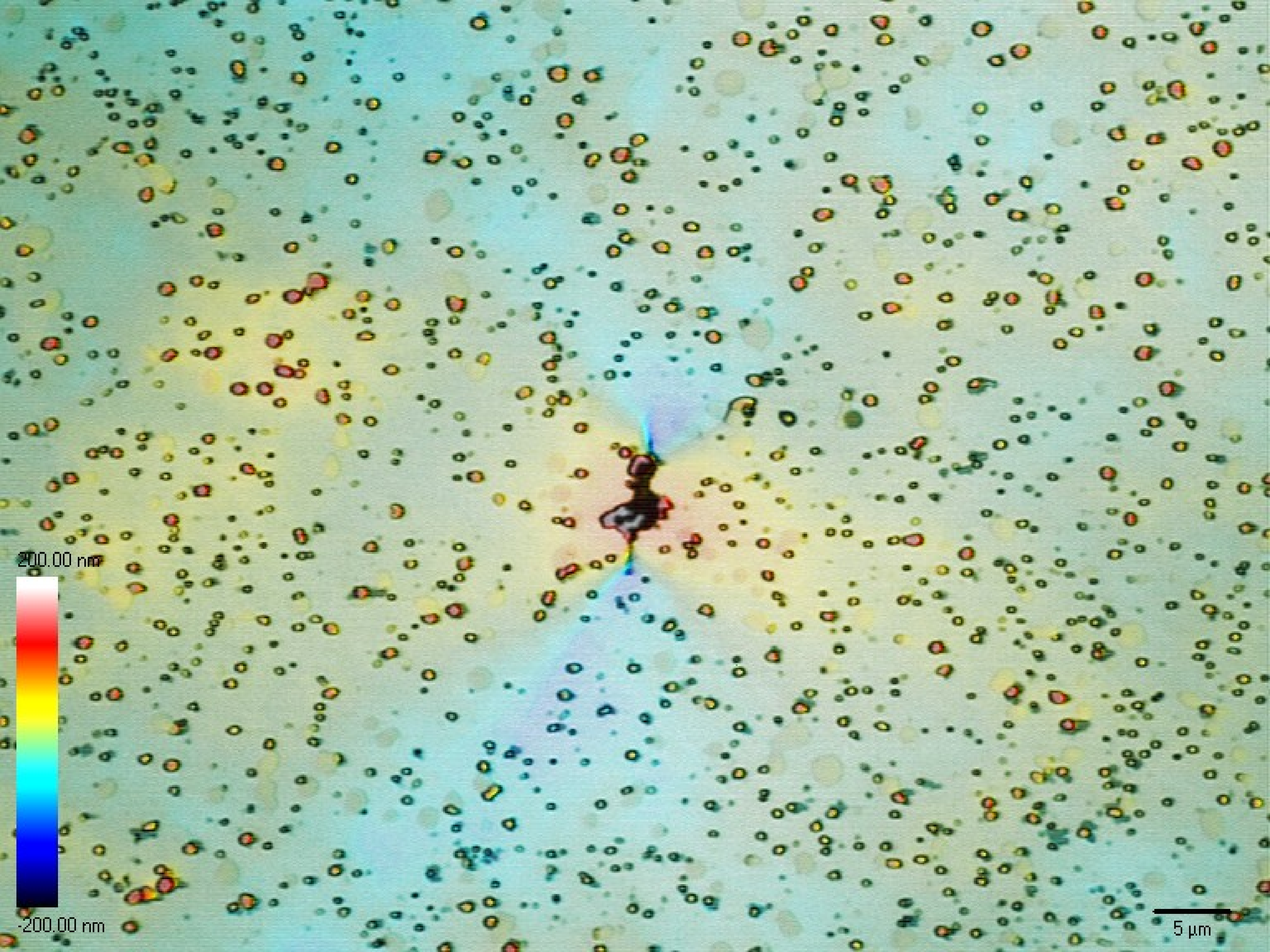
200.00 nm
-200.00 nm
5 µm

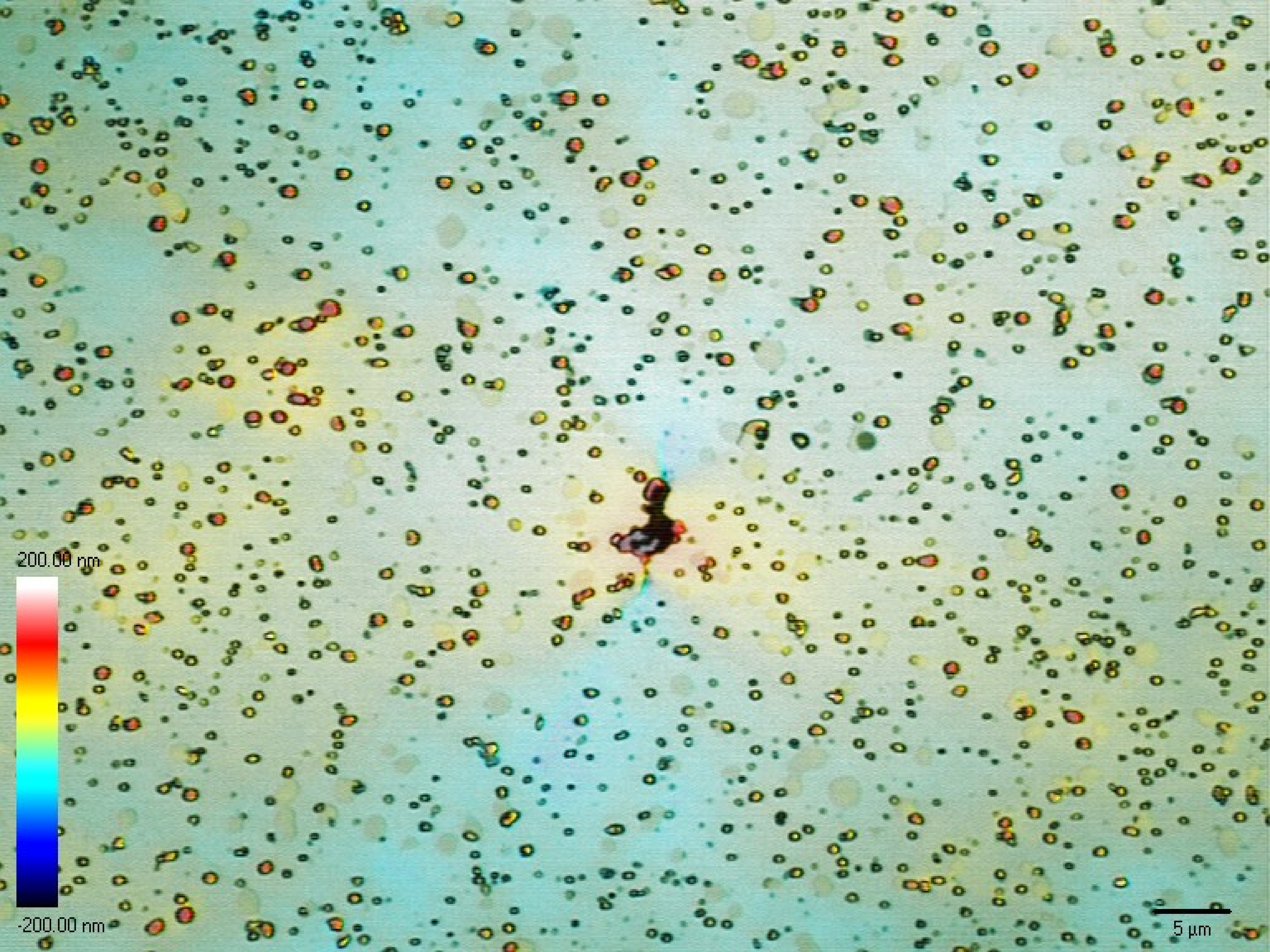
200.00 nm
-200.00 nm
5 µm

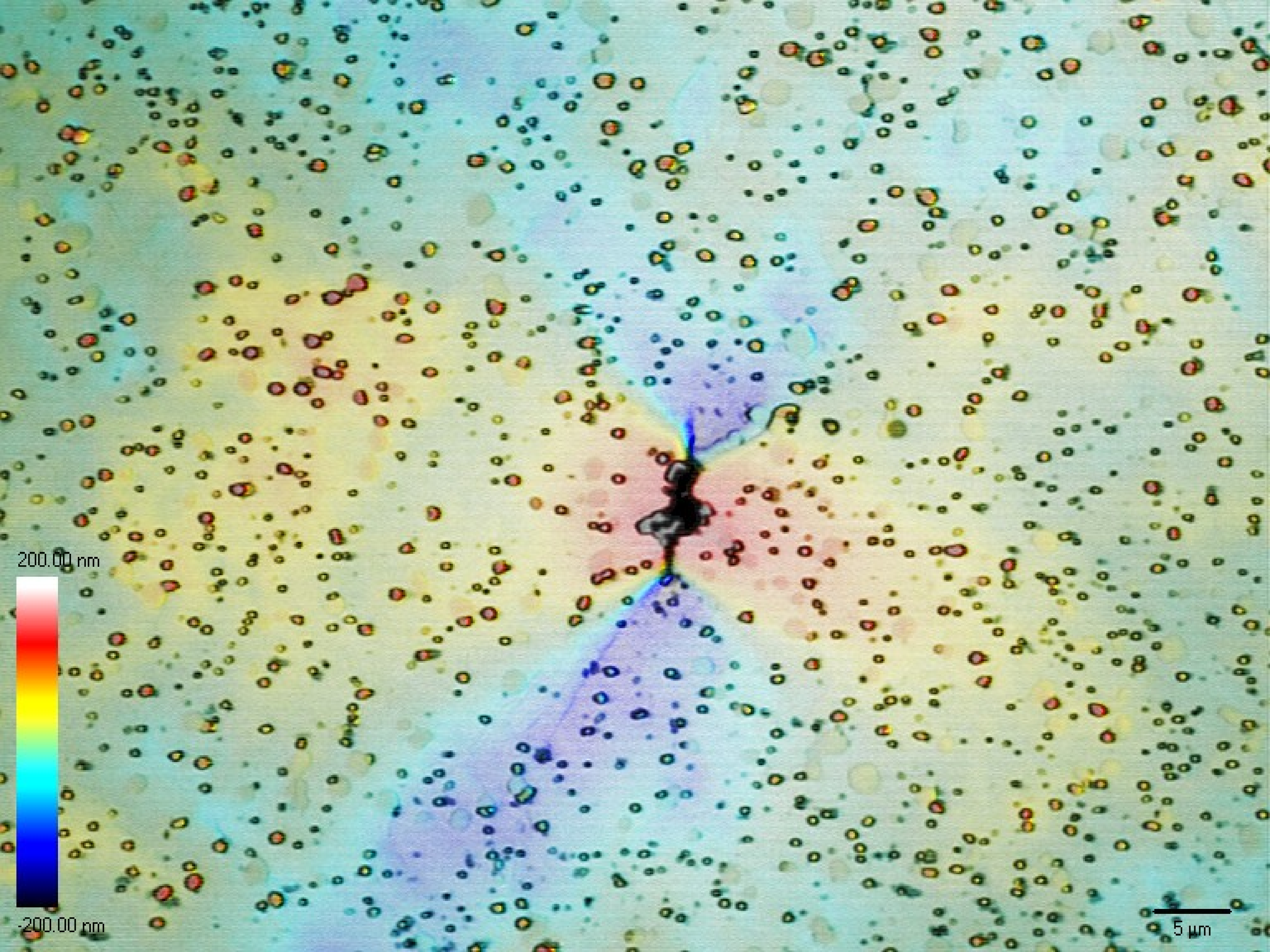
200.00 nm
-200.00 nm
5 µm

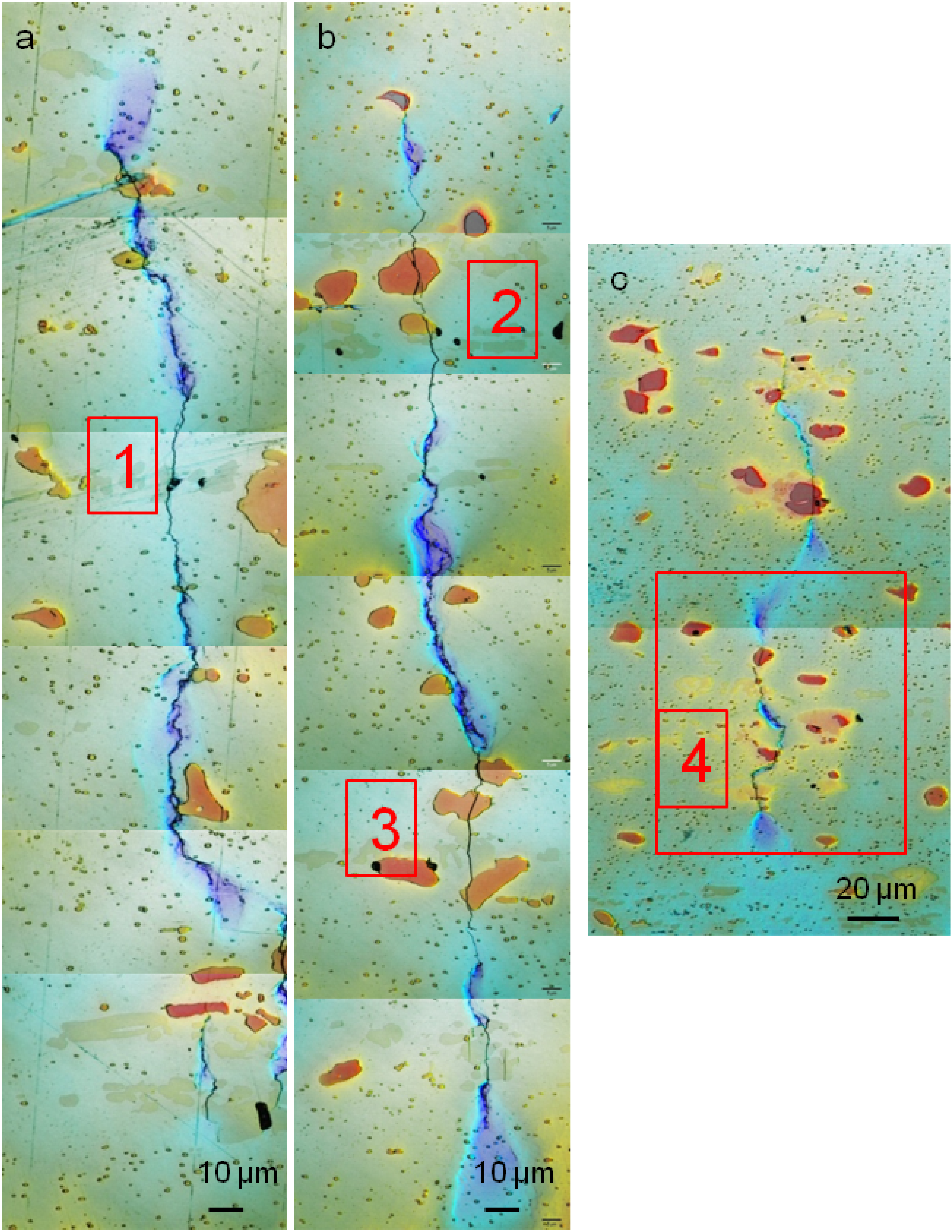
a
1
10 µm
b
2
3
10 µm
c
4
20 µm

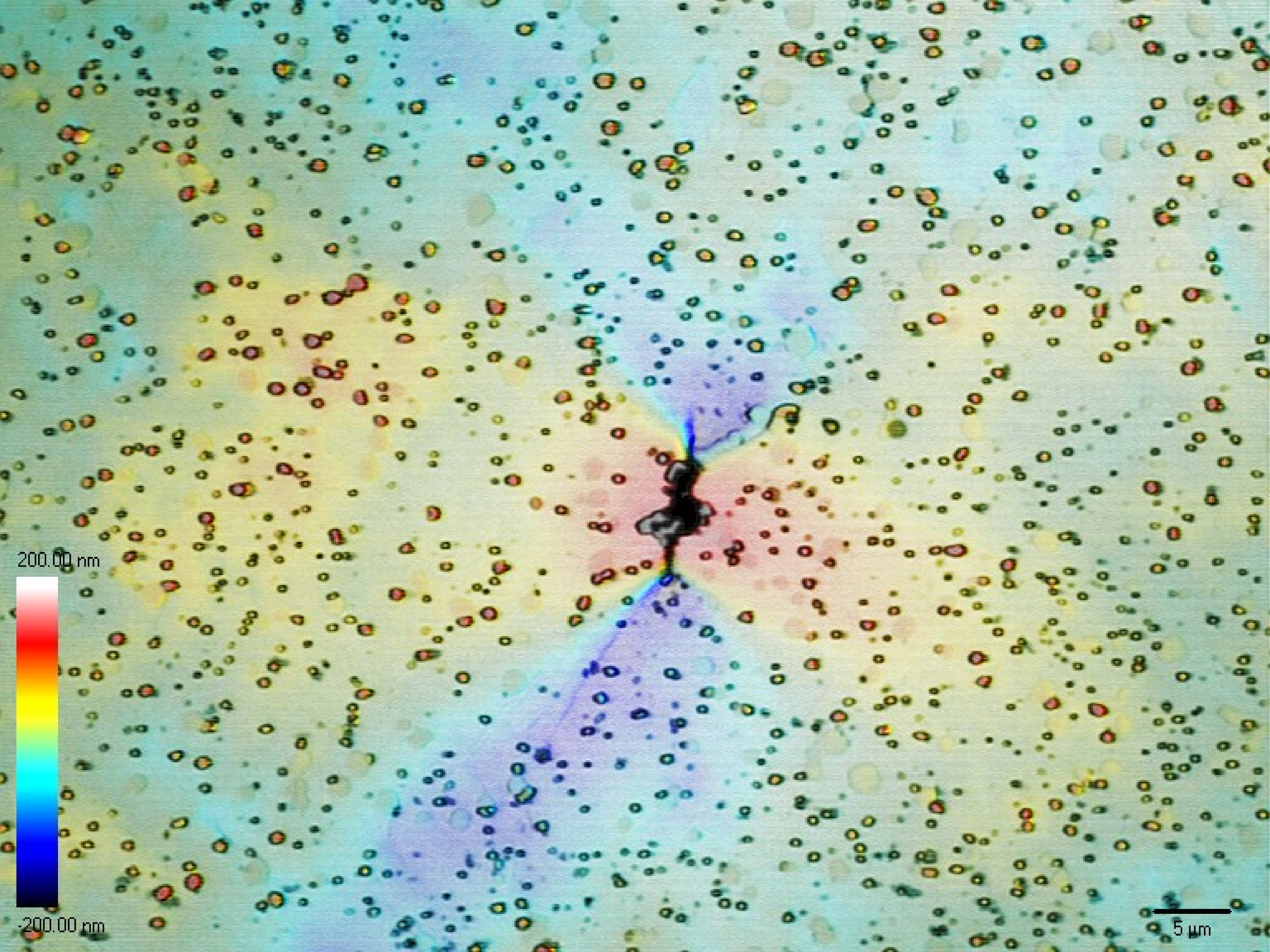
200.00 nm
-200.00 nm
5 µm

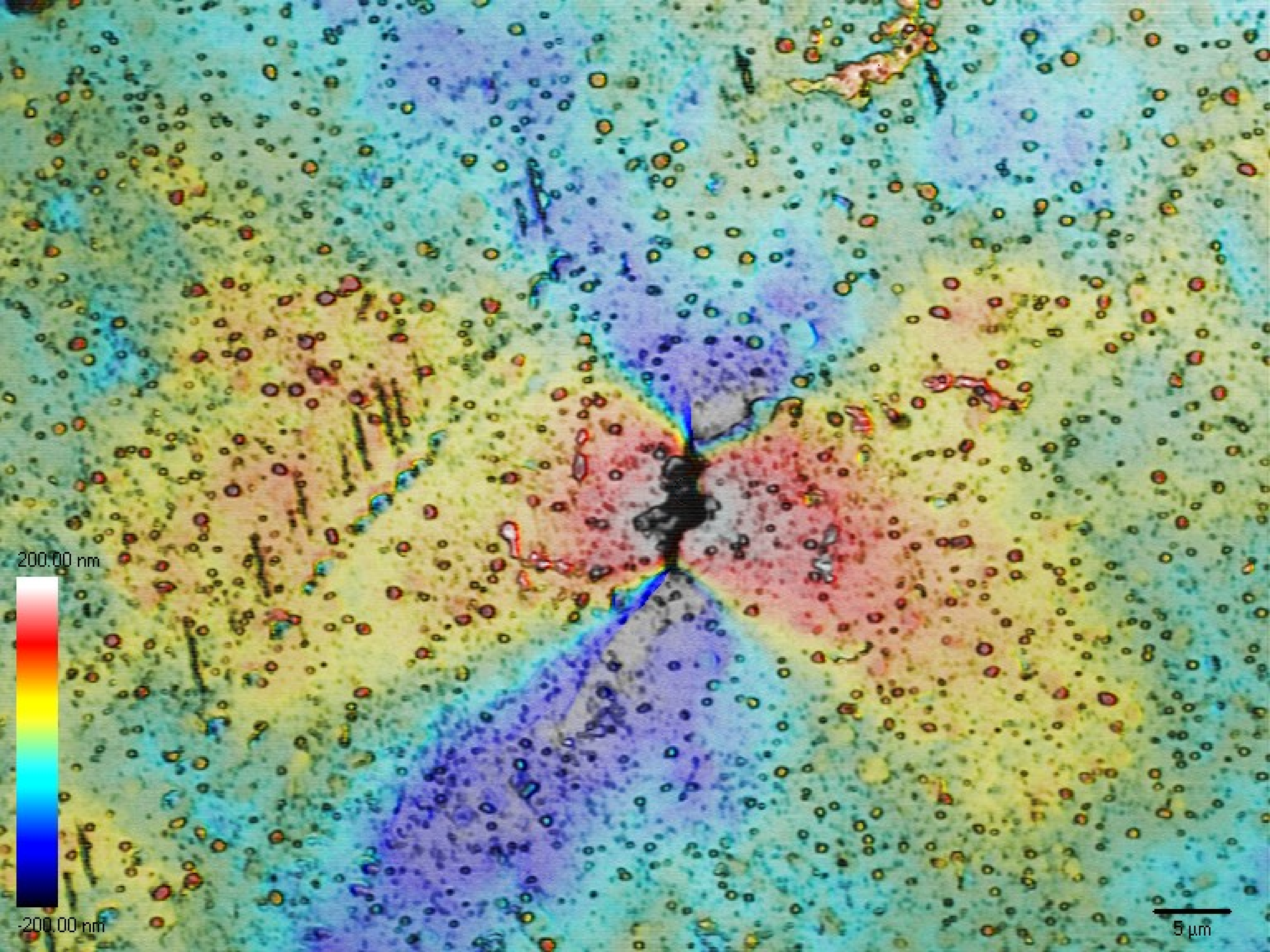
200.00 nm
-200.00 nm
5 µm

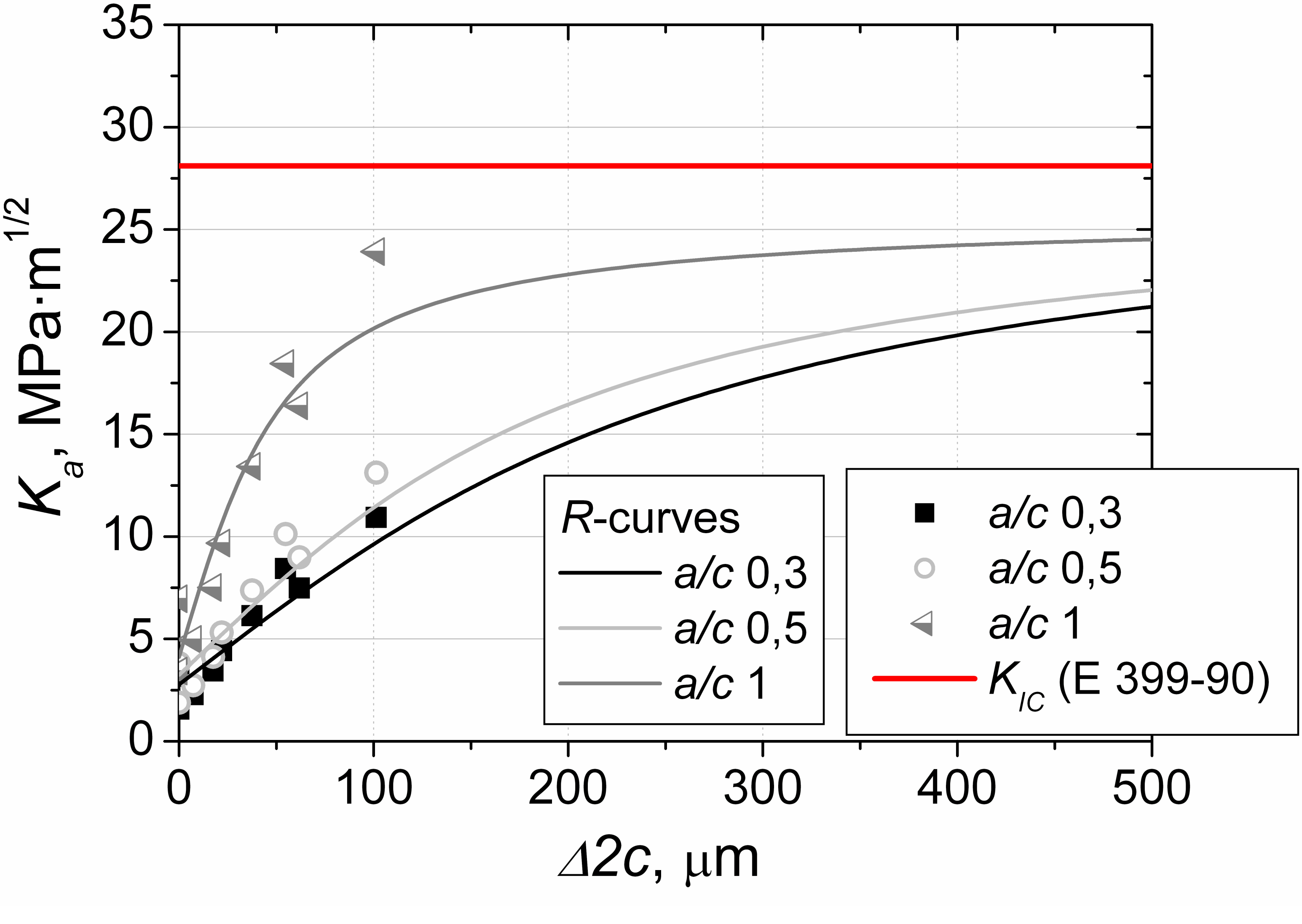

K_a, MPa·m$^{1/2}$
0
5
10
15
20
25
30
35
0
100
200
300
400
500
$\Delta 2c$, μm
R-curves
a/c 0,3
a/c 0,5
a/c 1
a/c 0,3
a/c 0,5
a/c 1
K_{IC} (E 399-90)

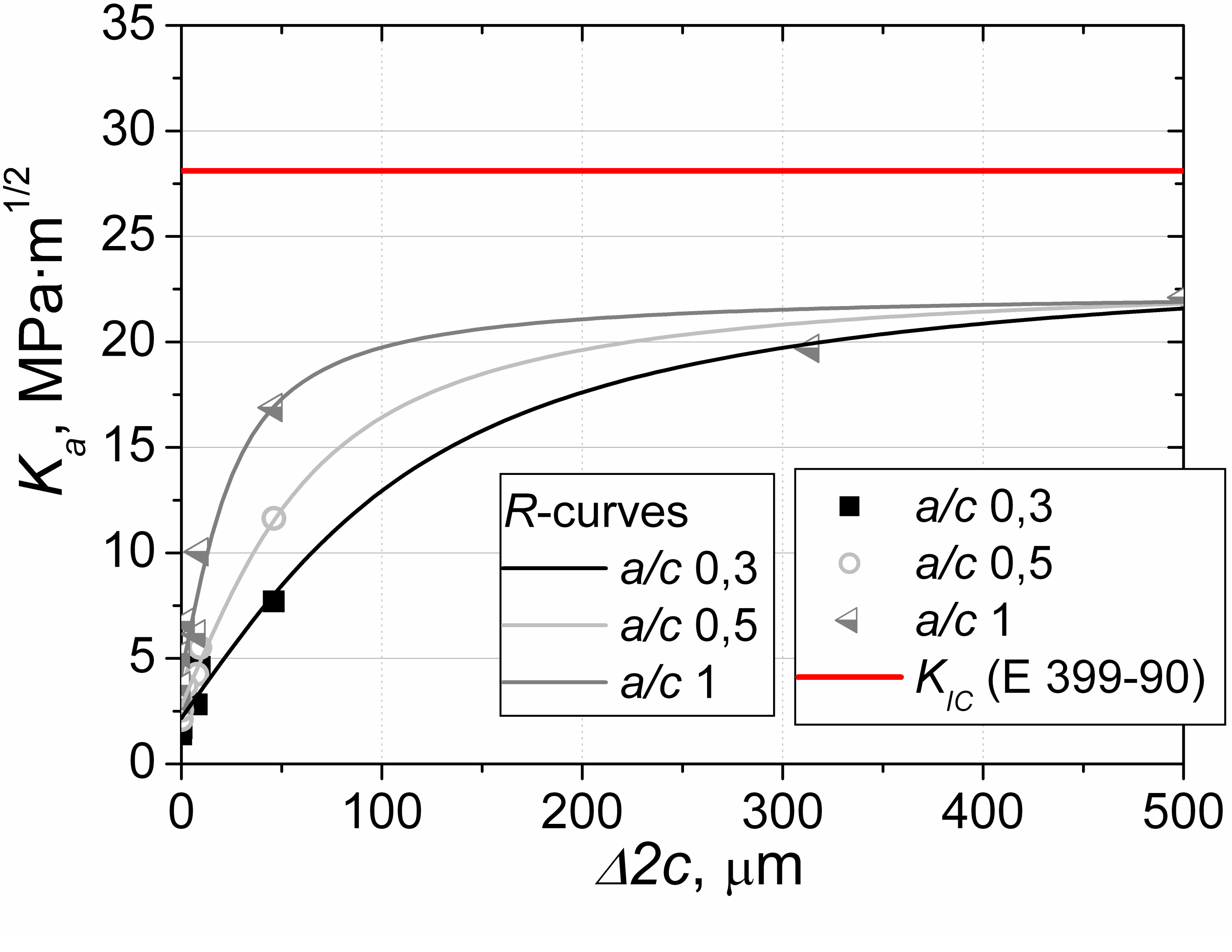
K_a, MPa·m$^{1/2}$
$\Delta 2c$, μm
0
5
10
15
20
25
30
35
0
100
200
300
400
500
R-curves
a/c 0,3
a/c 0,5
a/c 1
a/c 0,3
a/c 0,5
a/c 1
K_{IC} (E 399-90)

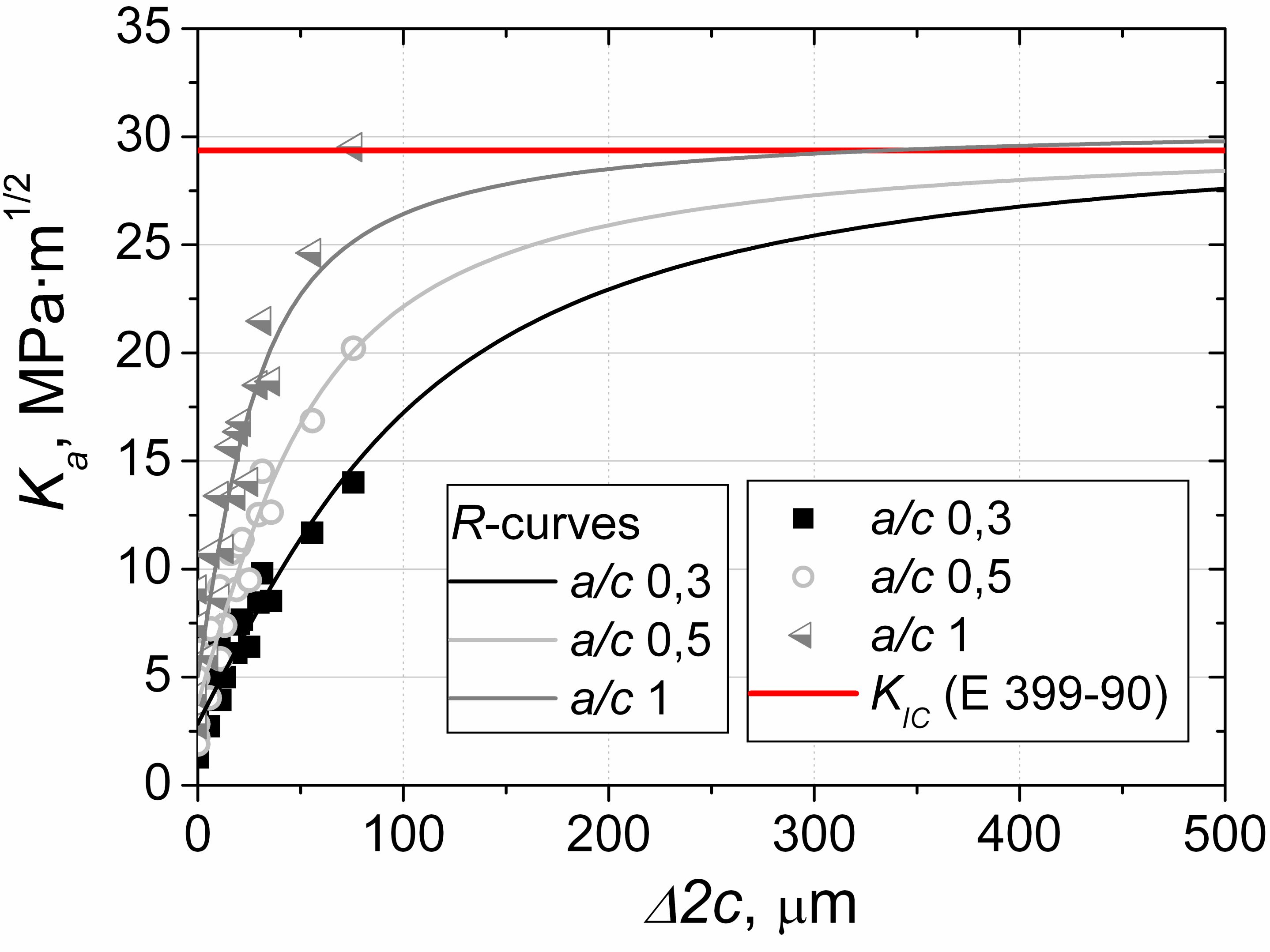

K_a, MPa·m$^{1/2}$
35
30
25
20
15
10
5
0
0
100
200
300
400
500
$\Delta 2c$, μm
R-curves
a/c 0,3
a/c 0,5
a/c 1
■ a/c 0,3
○ a/c 0,5
◁ a/c 1
K_{IC} (E 399-90)

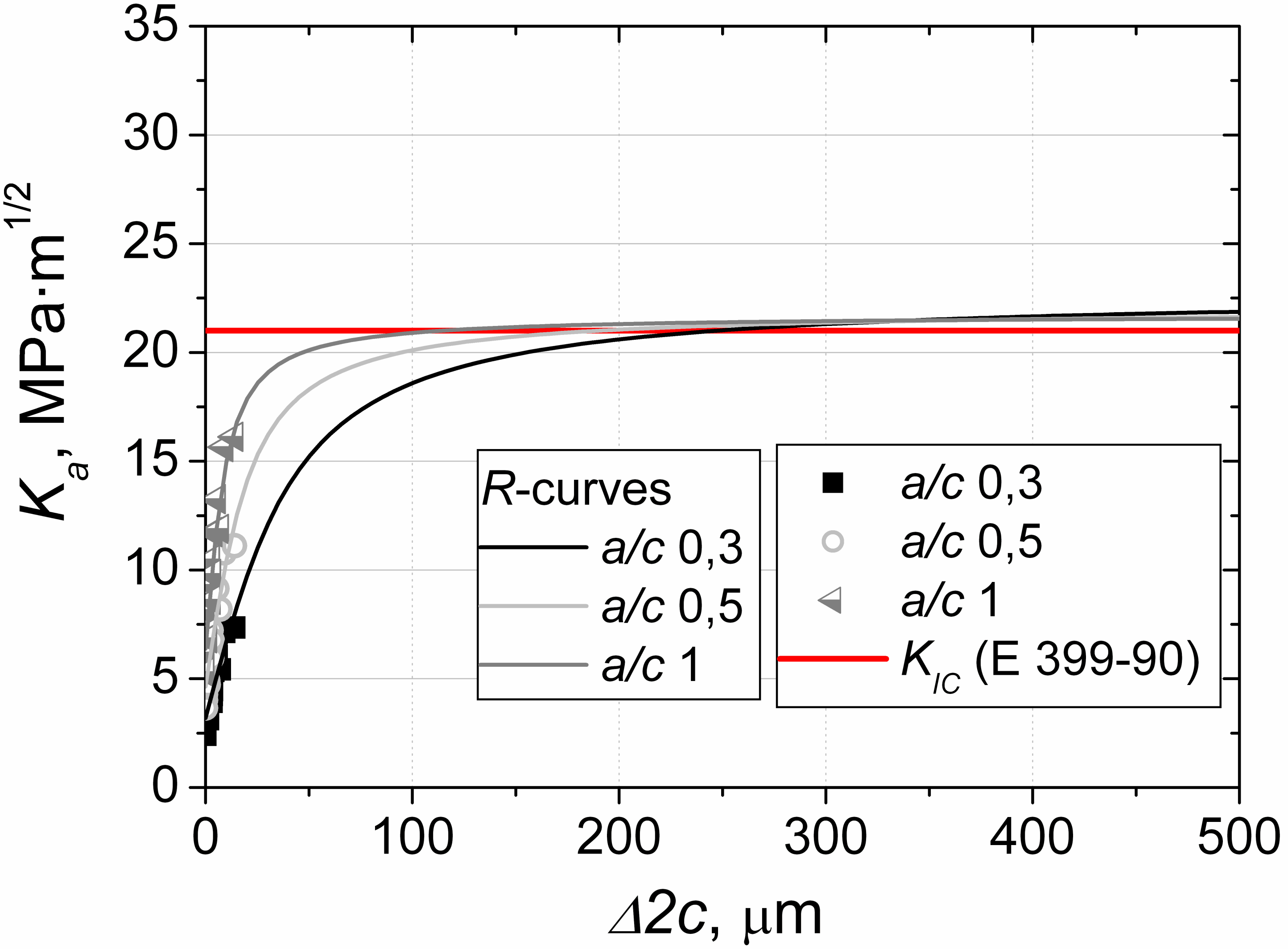

K_a, MPa·m$^{1/2}$
0
5
10
15
20
25
30
35
0
100
200
300
400
500
$\Delta 2c$, μm
R-curves
a/c 0,3
a/c 0,5
a/c 1
a/c 0,3
a/c 0,5
a/c 1
K_{IC} (E 399-90)

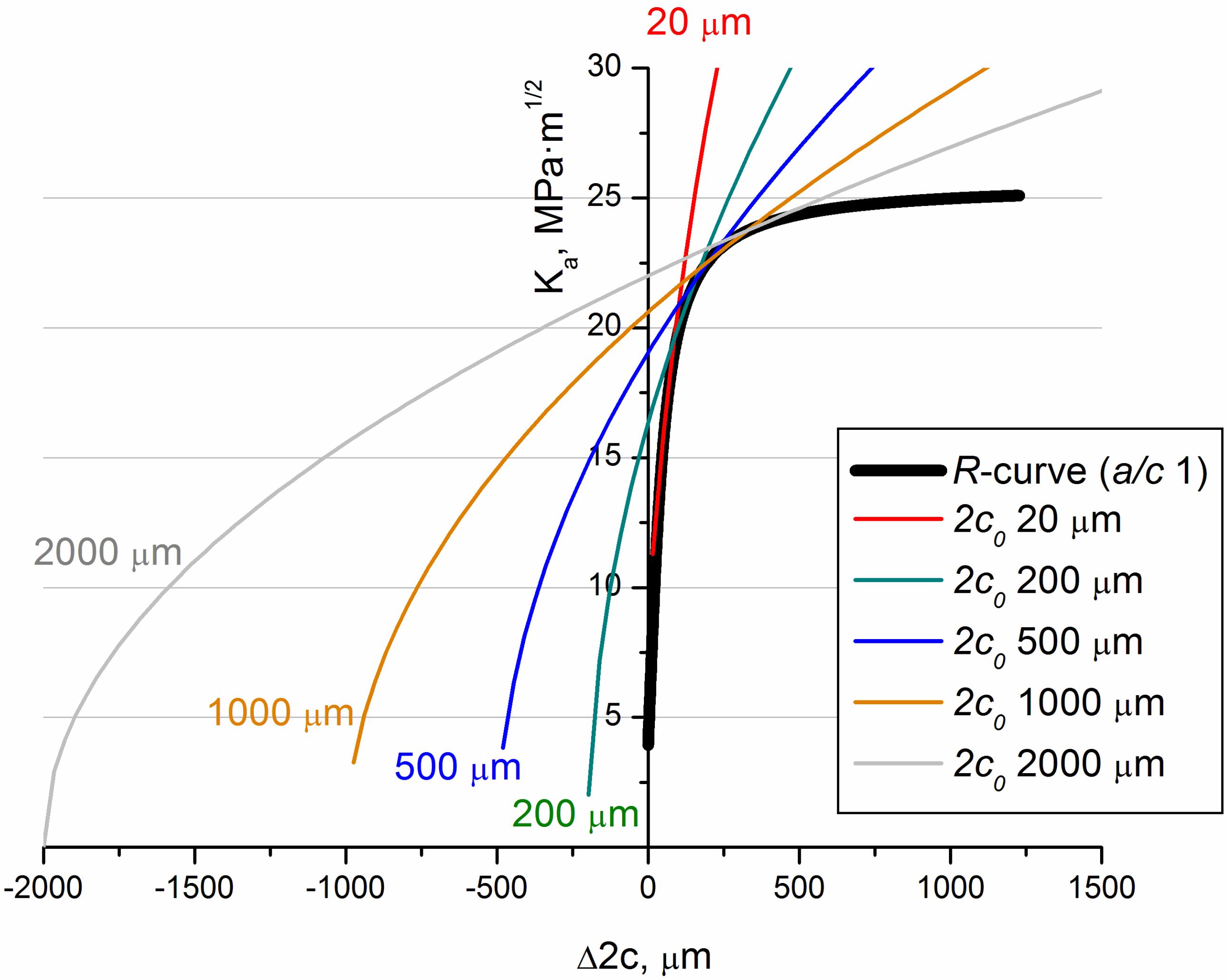
20 μm
2000 μm
1000 μm
500 μm
200 μm
K_a, MPa·m$^{1/2}$
30
25
20
15
10
5
-2000
-1500
-1000
-500
0
500
1000
1500
Δ2c, μm
R-curve (*a/c* 1)
2c₀ 20 μm
2c₀ 200 μm
2c₀ 500 μm
2c₀ 1000 μm
2c₀ 2000 μm

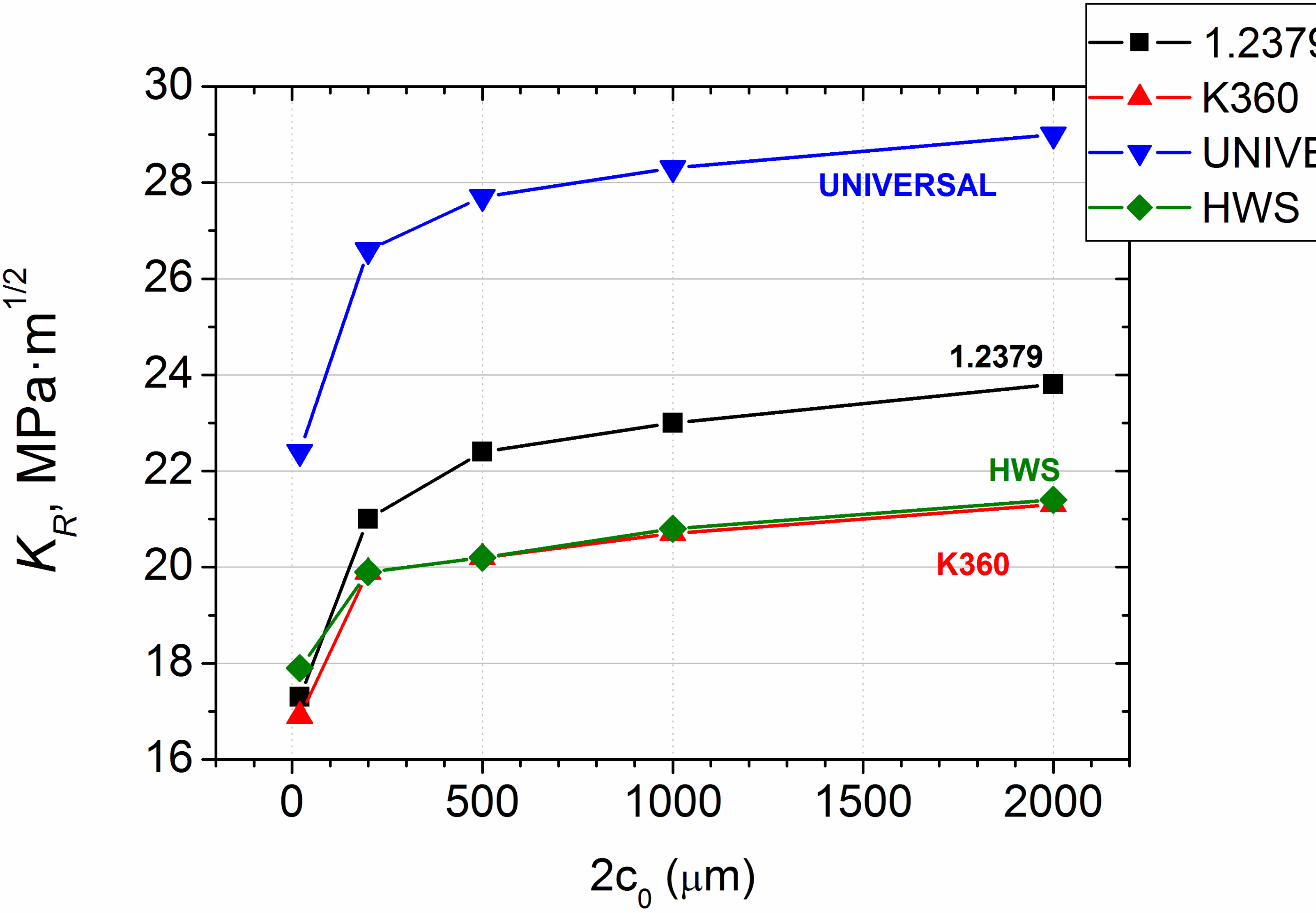

1.2379
K360
UNIVE
HWS
UNIVERSAL
1.2379
HWS
K360
K_R, MPa·m$^{1/2}$
16
18
20
22
24
26
28
30
0
500
1000
1500
2000
2c$_0$ (μm)

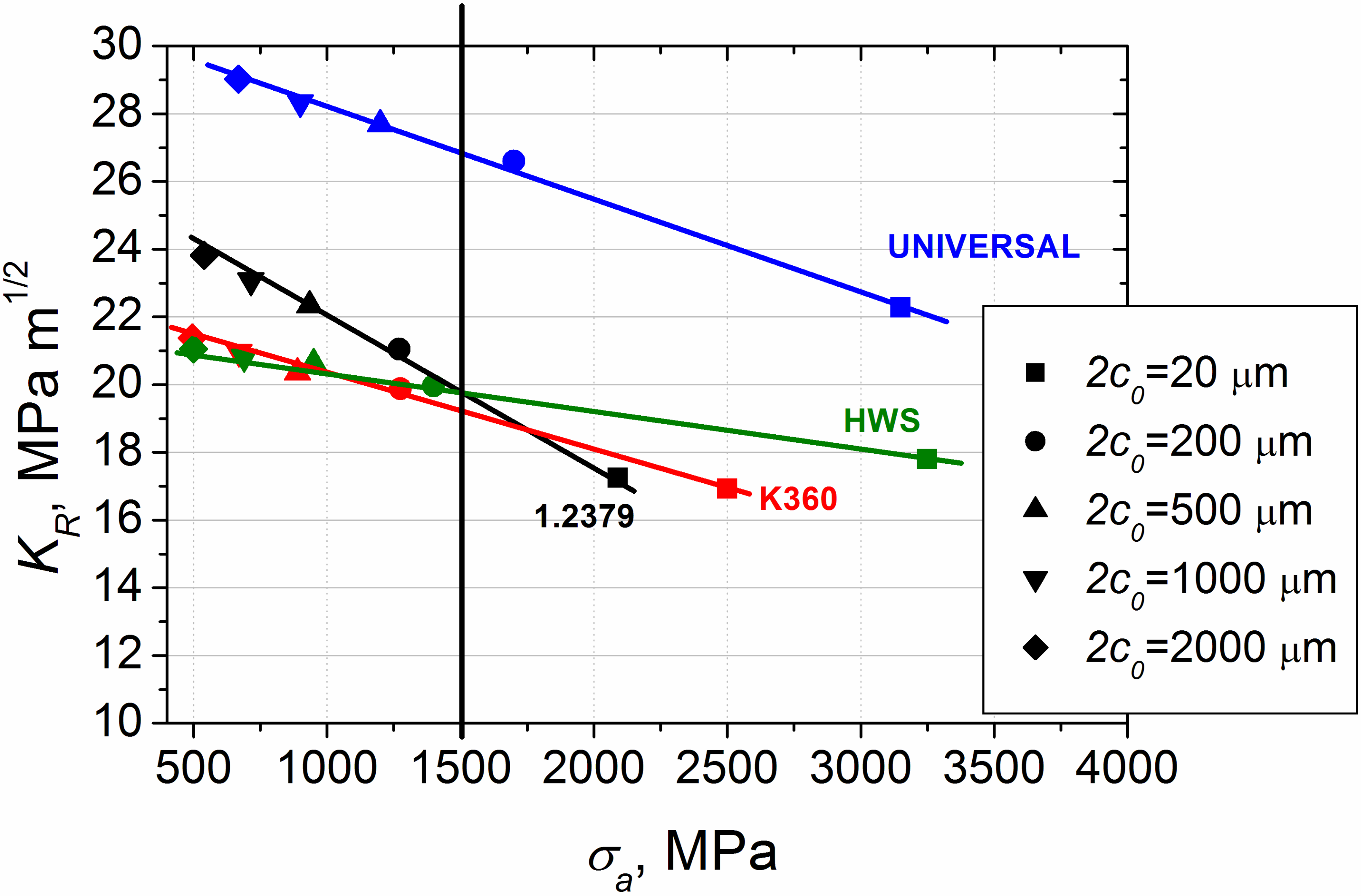
K_R, MPa m$^{1/2}$
30
28
26
24
22
20
18
16
14
12
10
500
1000
1500
2000
2500
3000
3500
4000
σ_a, MPa
UNIVERSAL
HWS
K360
1.2379
$2c_0$=20 μm
$2c_0$=200 μm
$2c_0$=500 μm
$2c_0$=1000 μm
$2c_0$=2000 μm

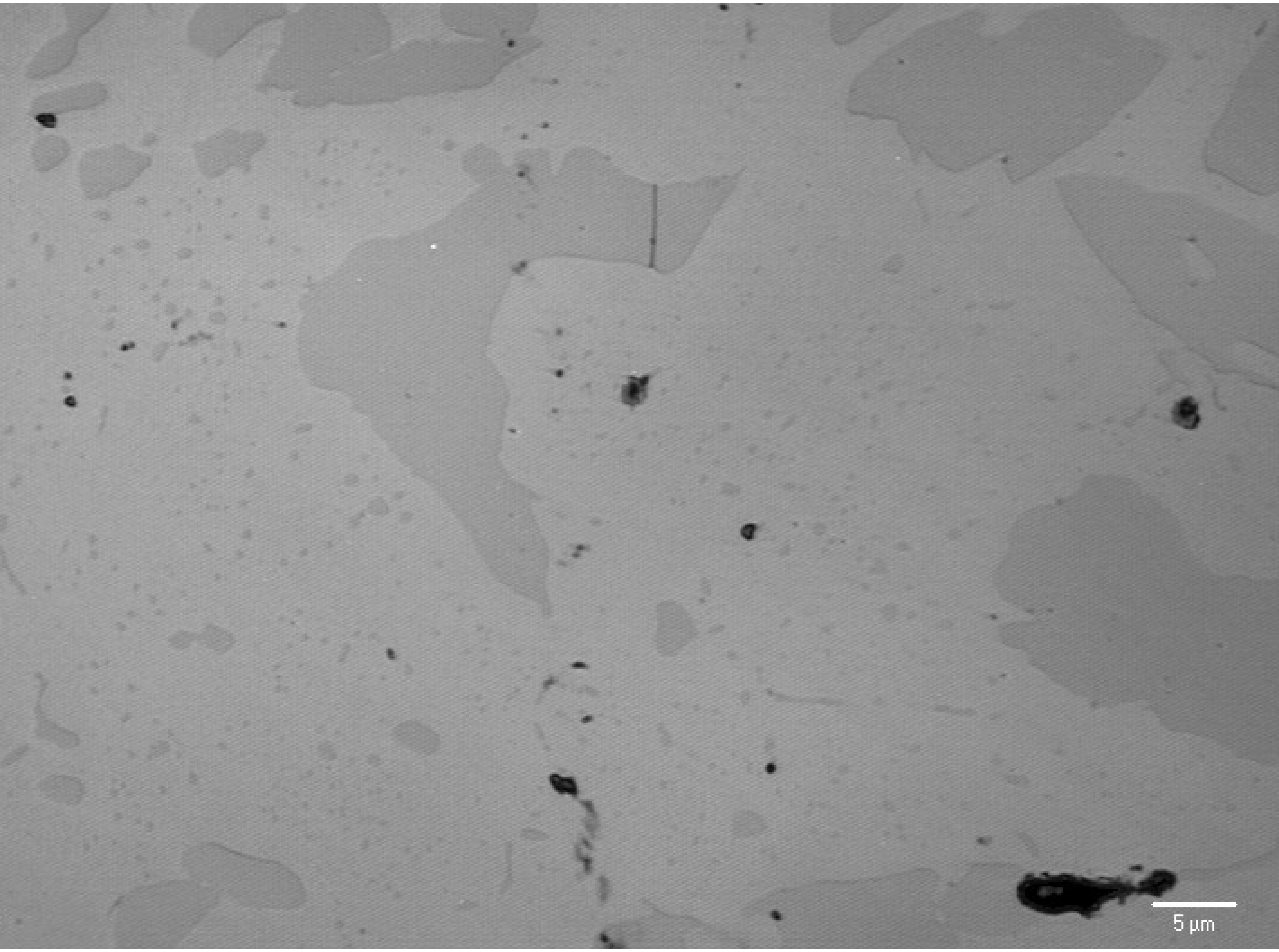
5 µm

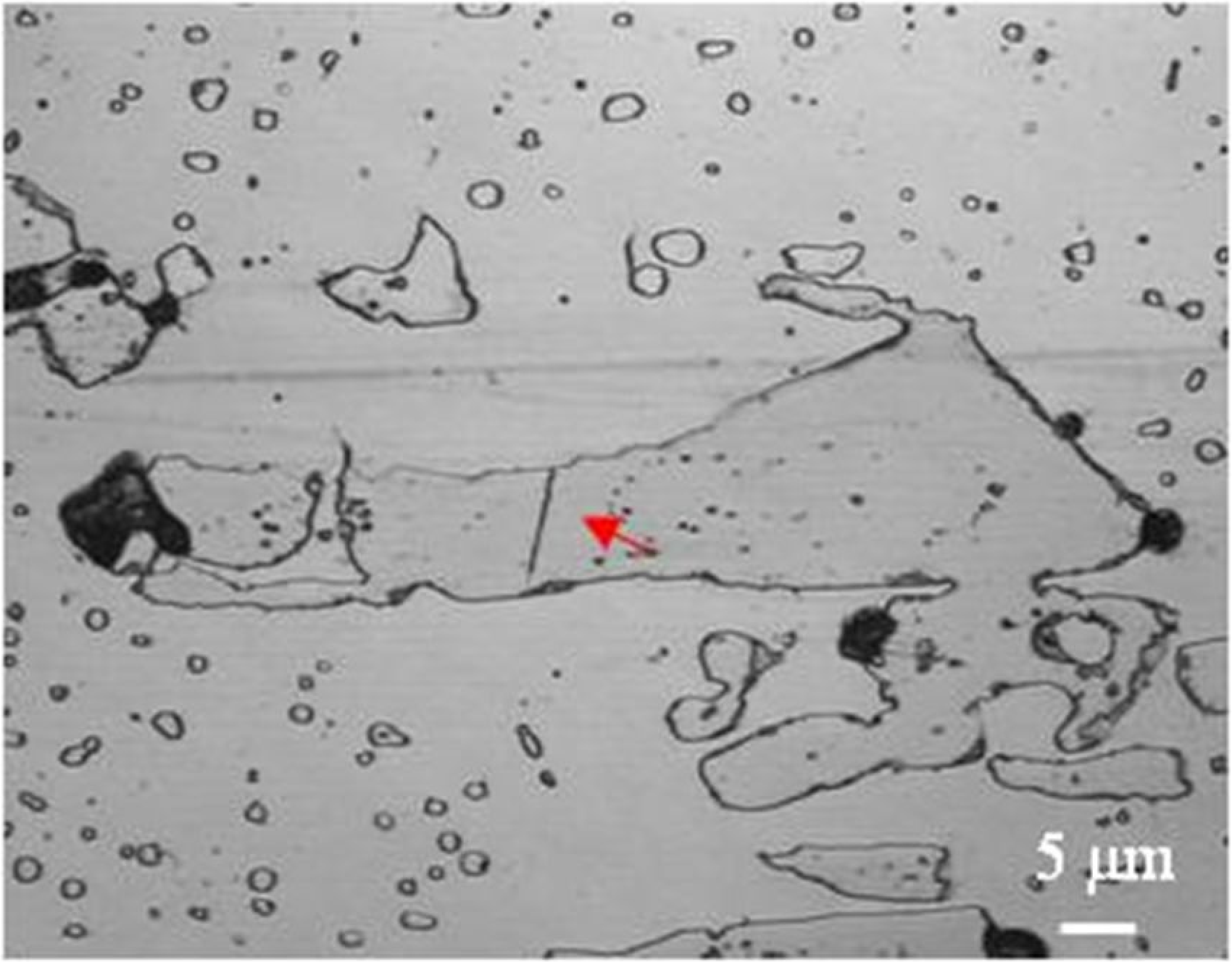
5 µm

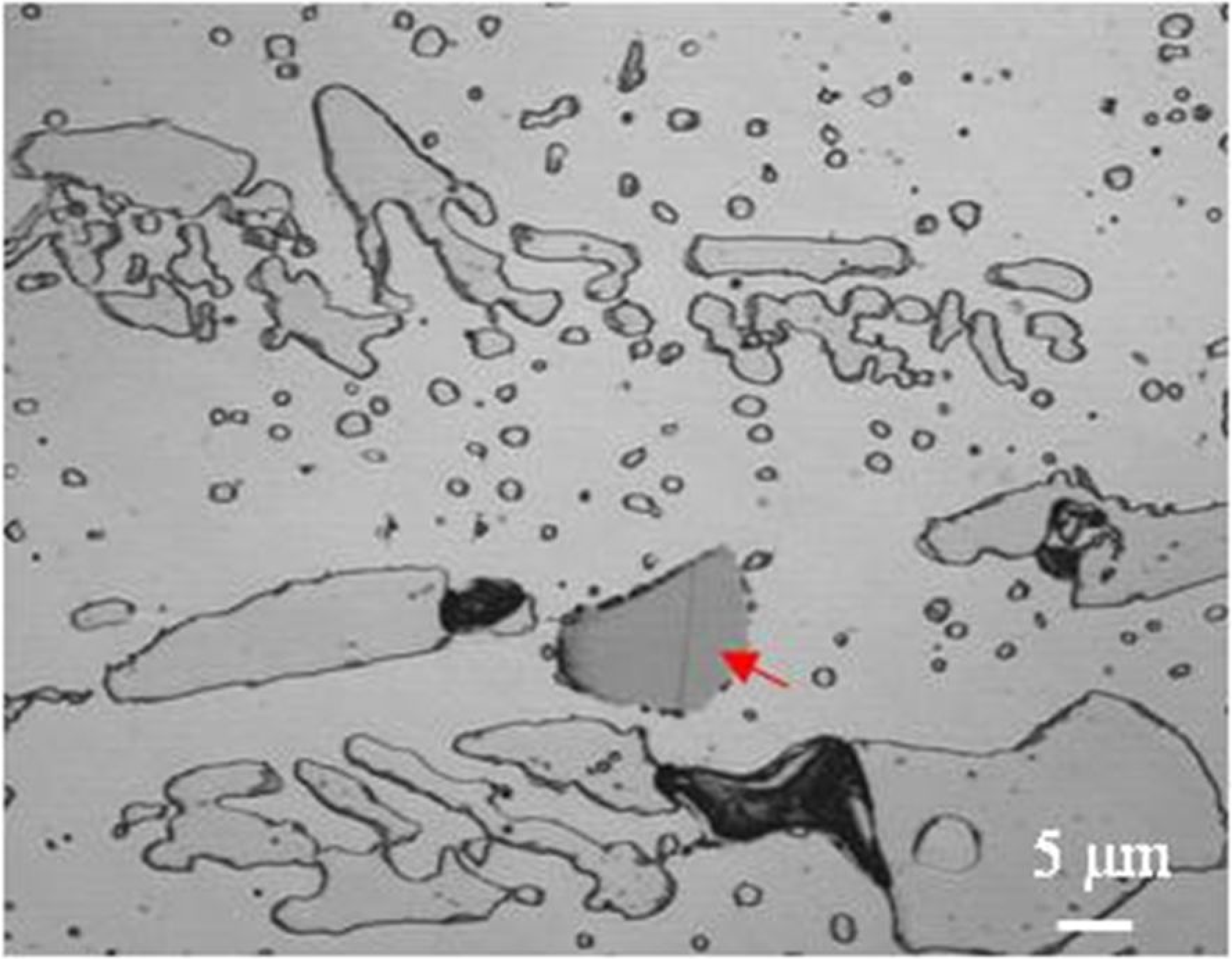
5 µm

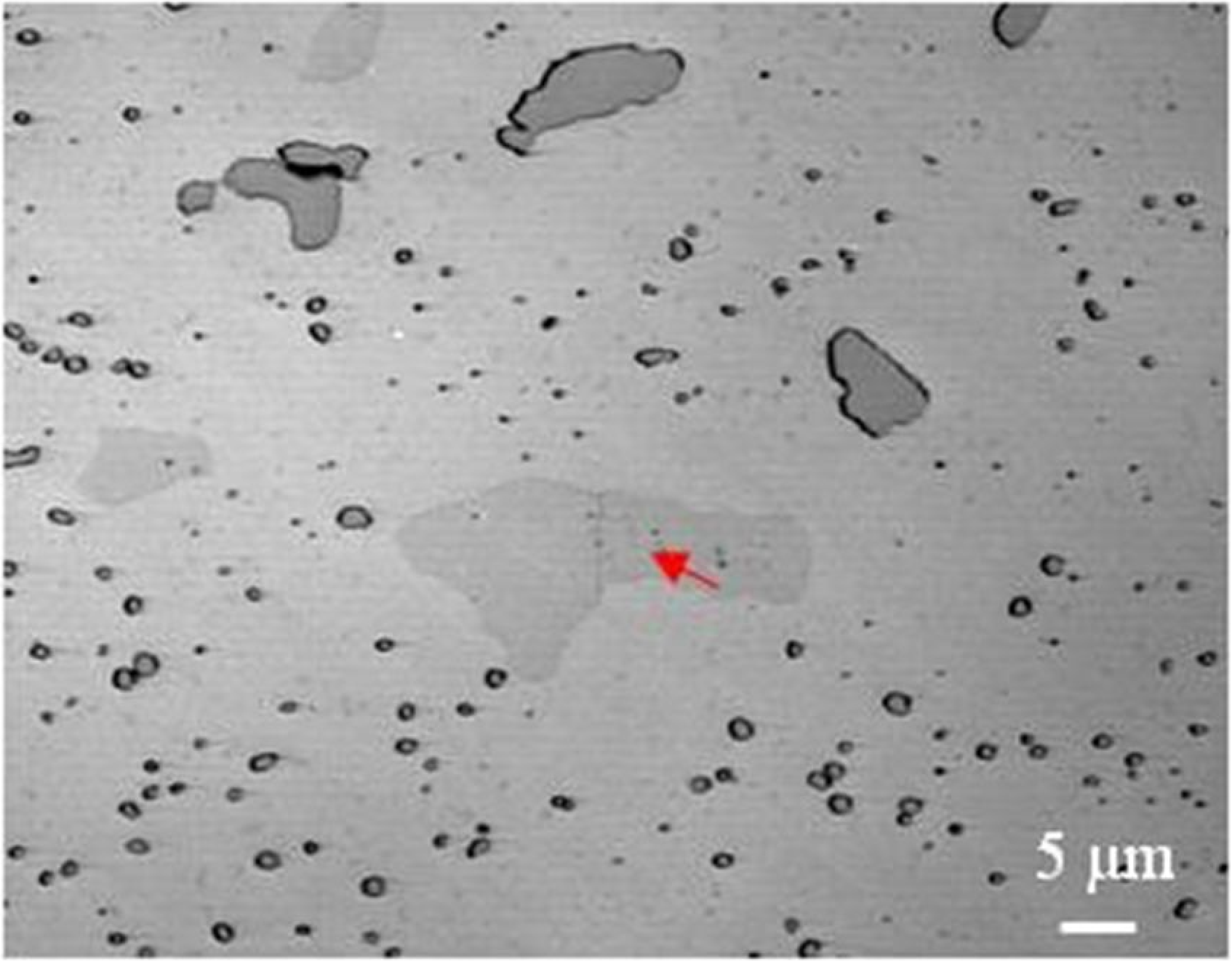
5 µm

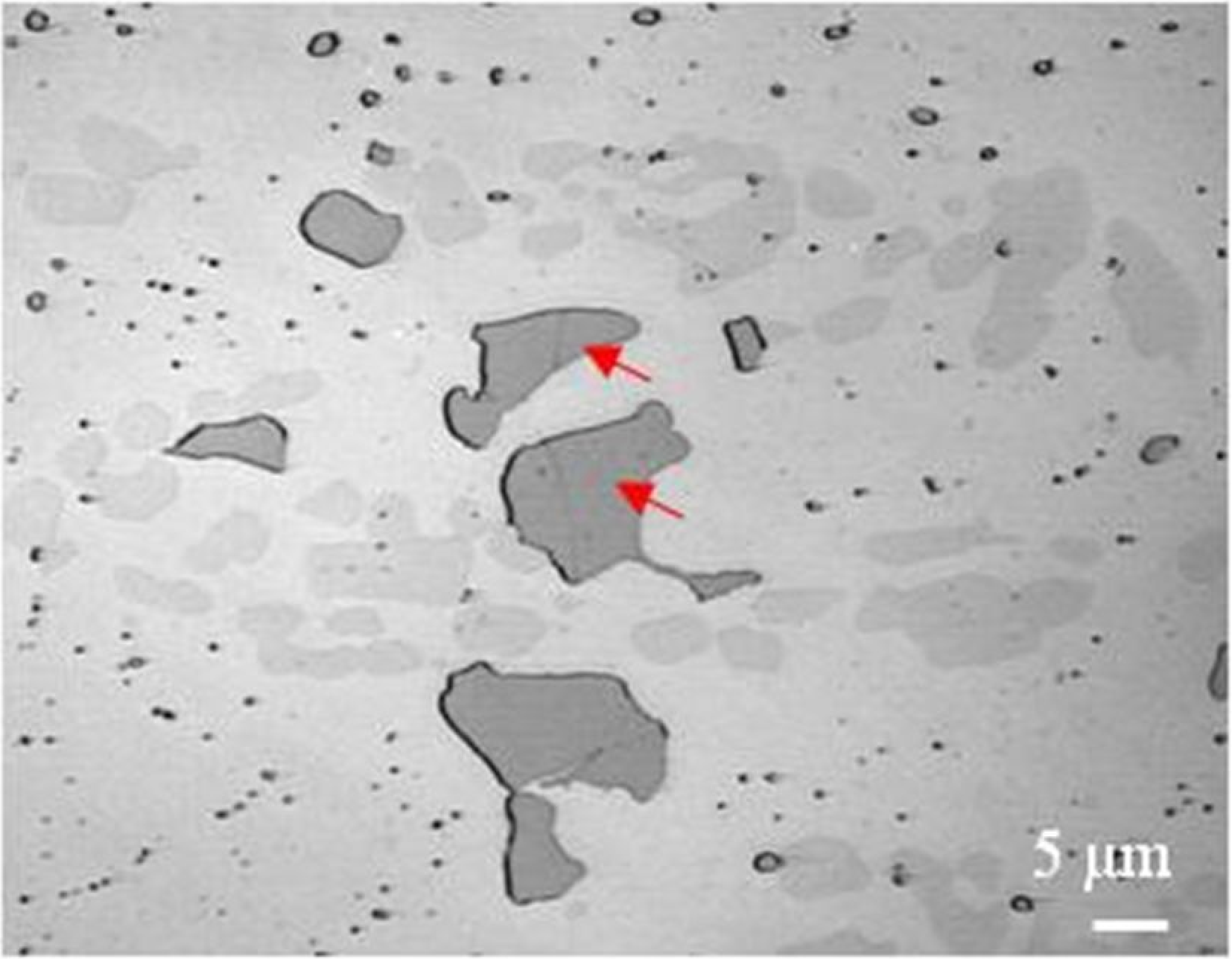
5 μm

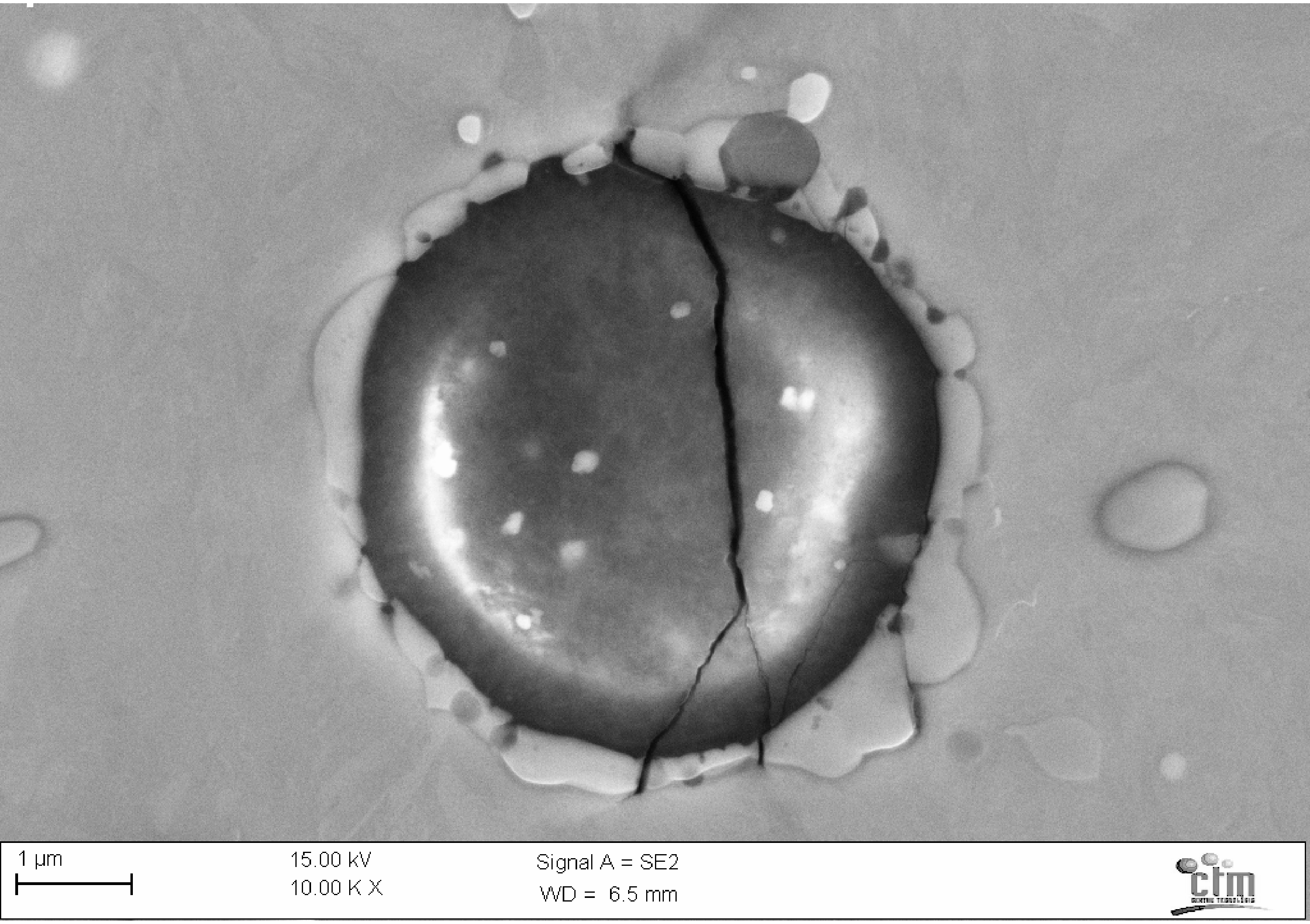
1 µm
15.00 kV
10.00 K X
Signal A = SE2
WD = 6.5 mm

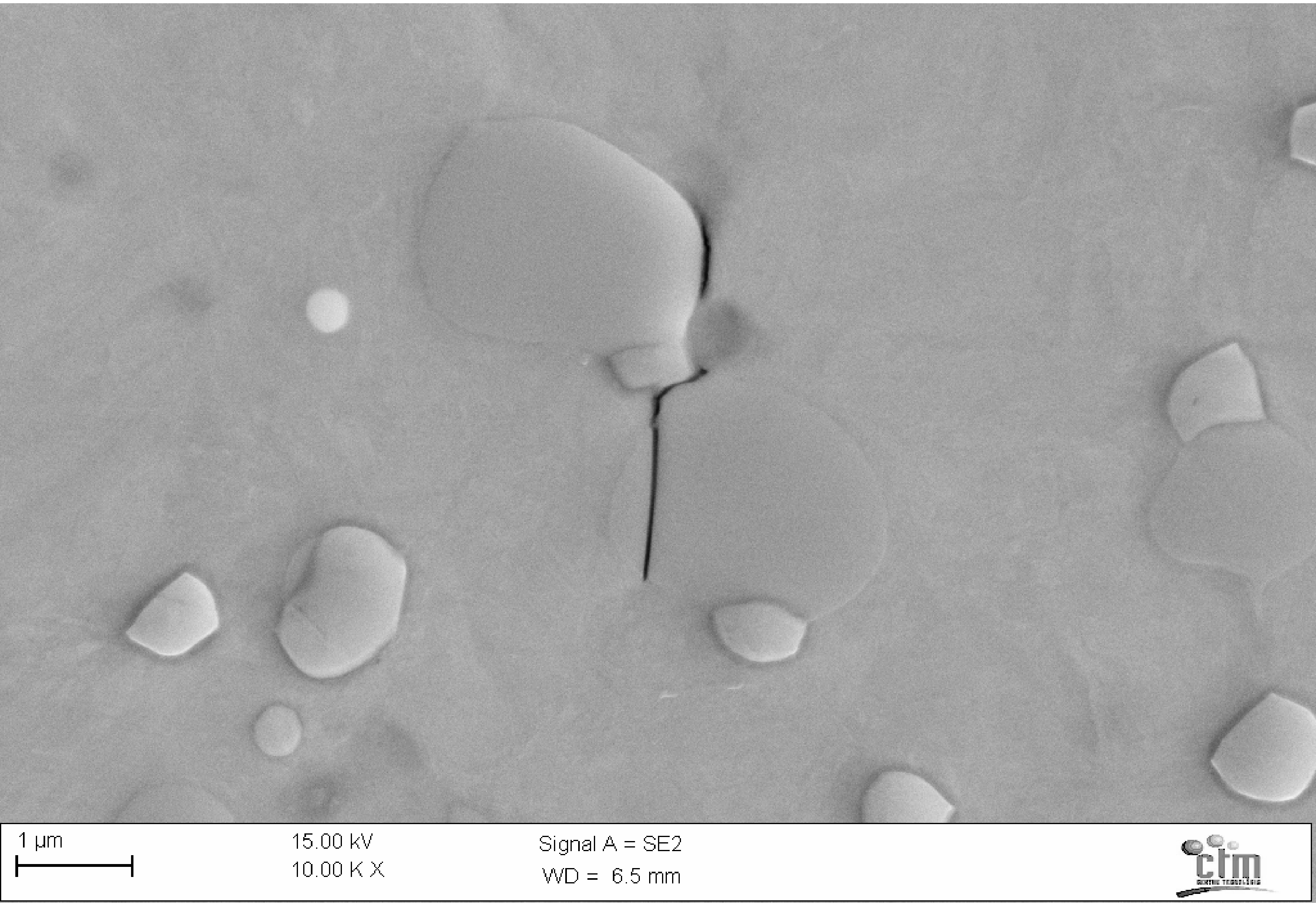
1 µm
15.00 kV
10.00 K X
Signal A = SE2
WD = 6.5 mm
ctm

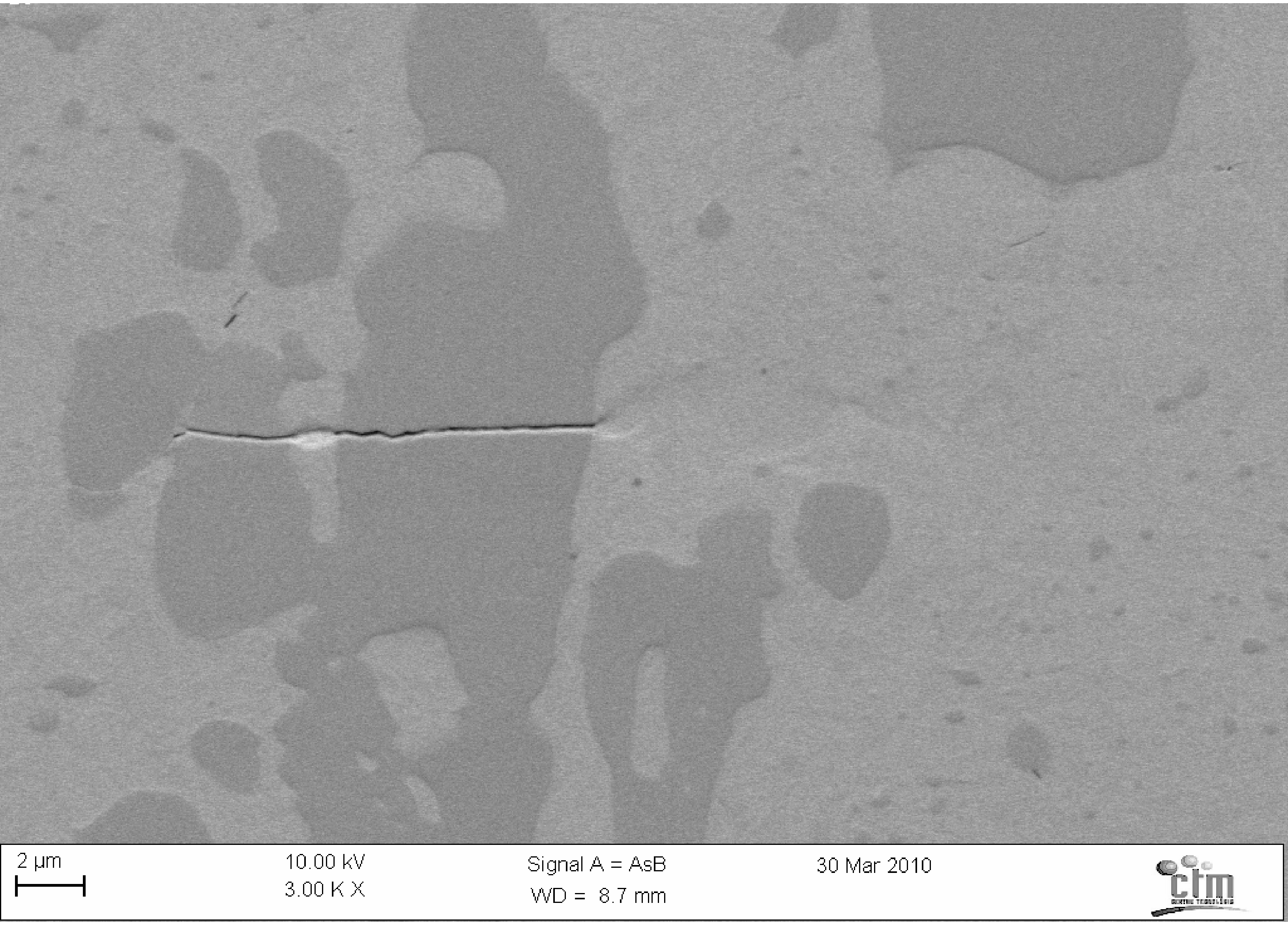
2 µm
10.00 kV
3.00 K X
Signal A = AsB
WD = 8.7 mm
30 Mar 2010
ctm

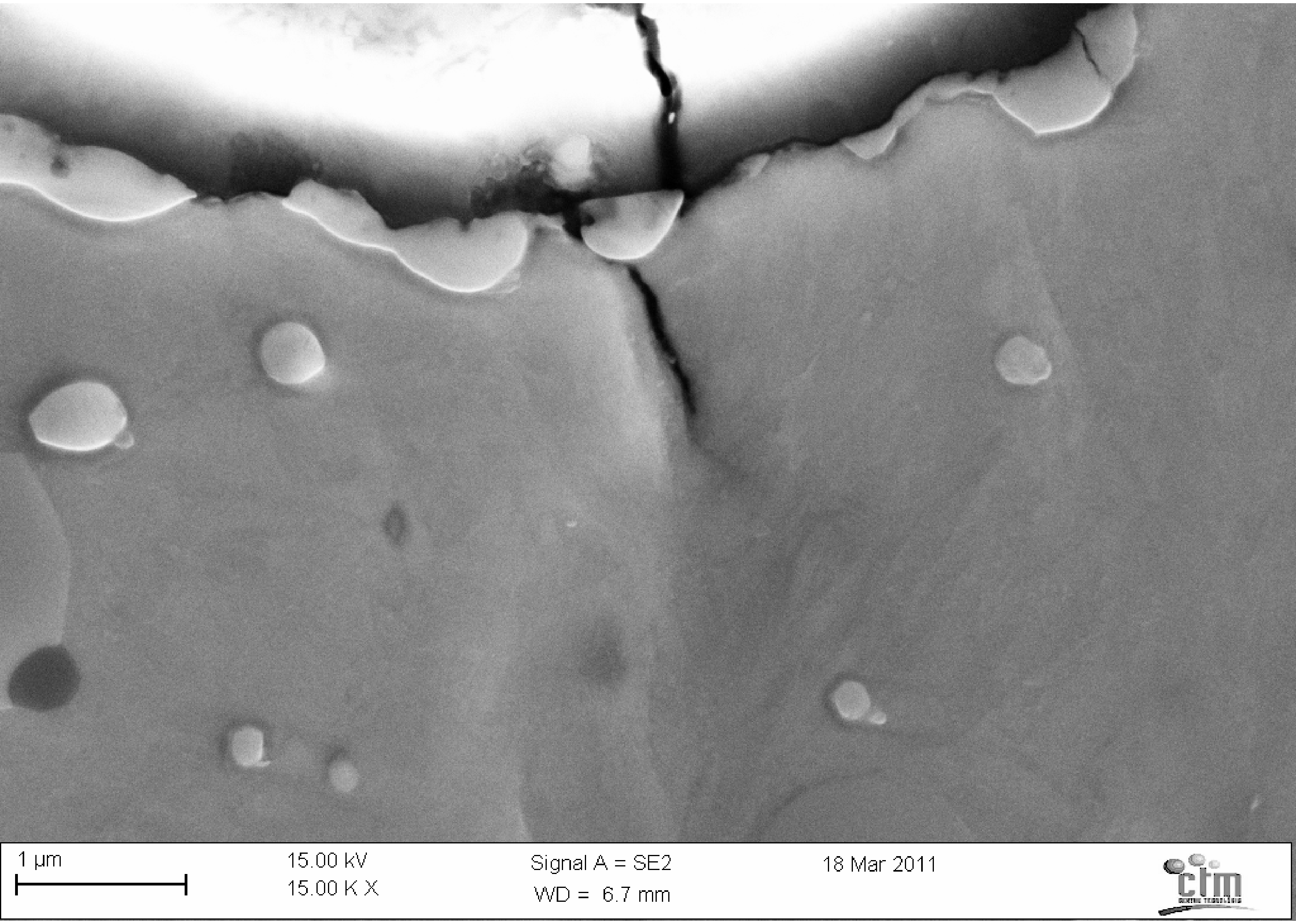
1 µm
15.00 kV
15.00 K X
Signal A = SE2
WD = 6.7 mm
18 Mar 2011
ctm

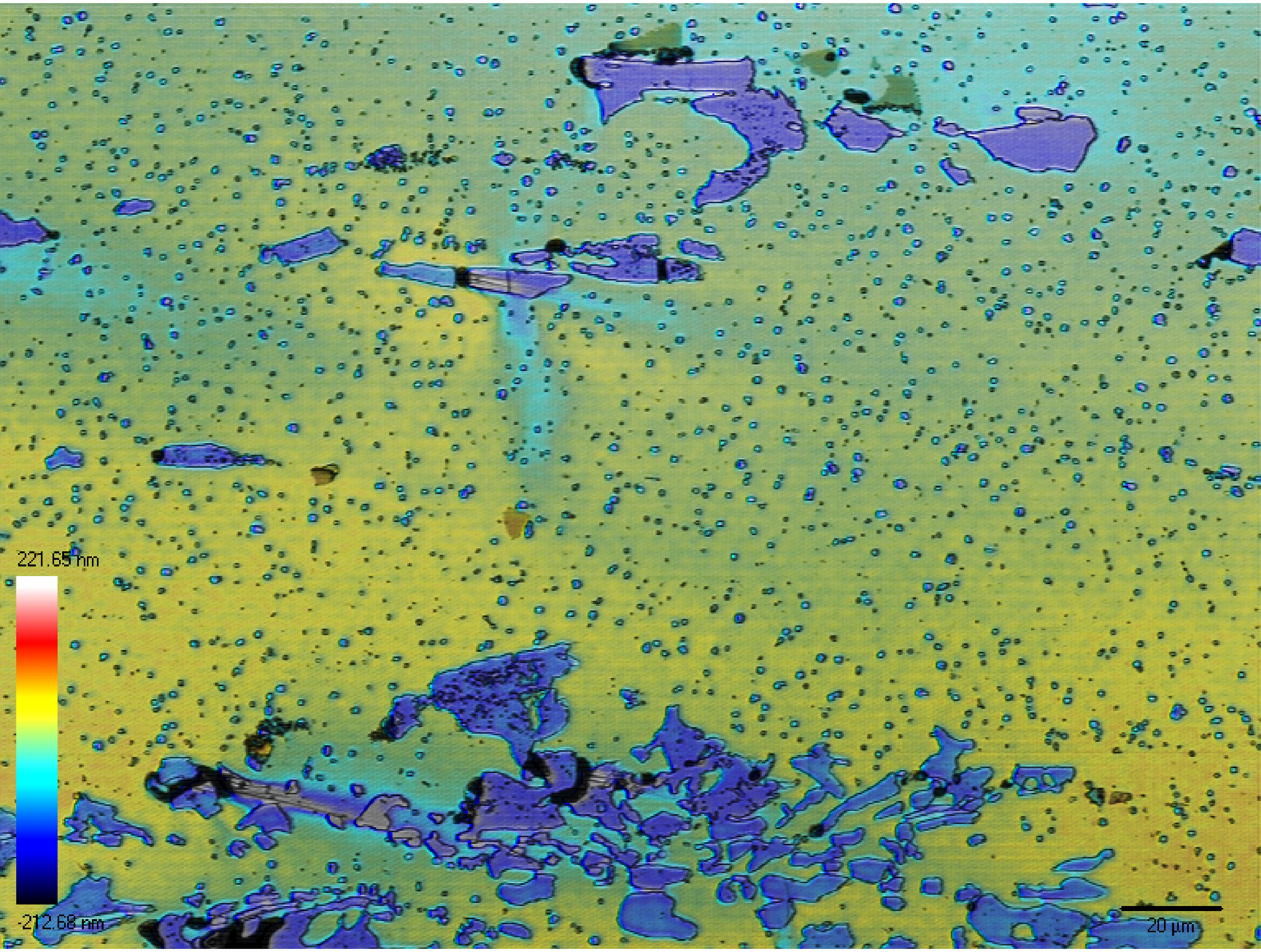
221.65 nm
-212.68 nm
20 µm

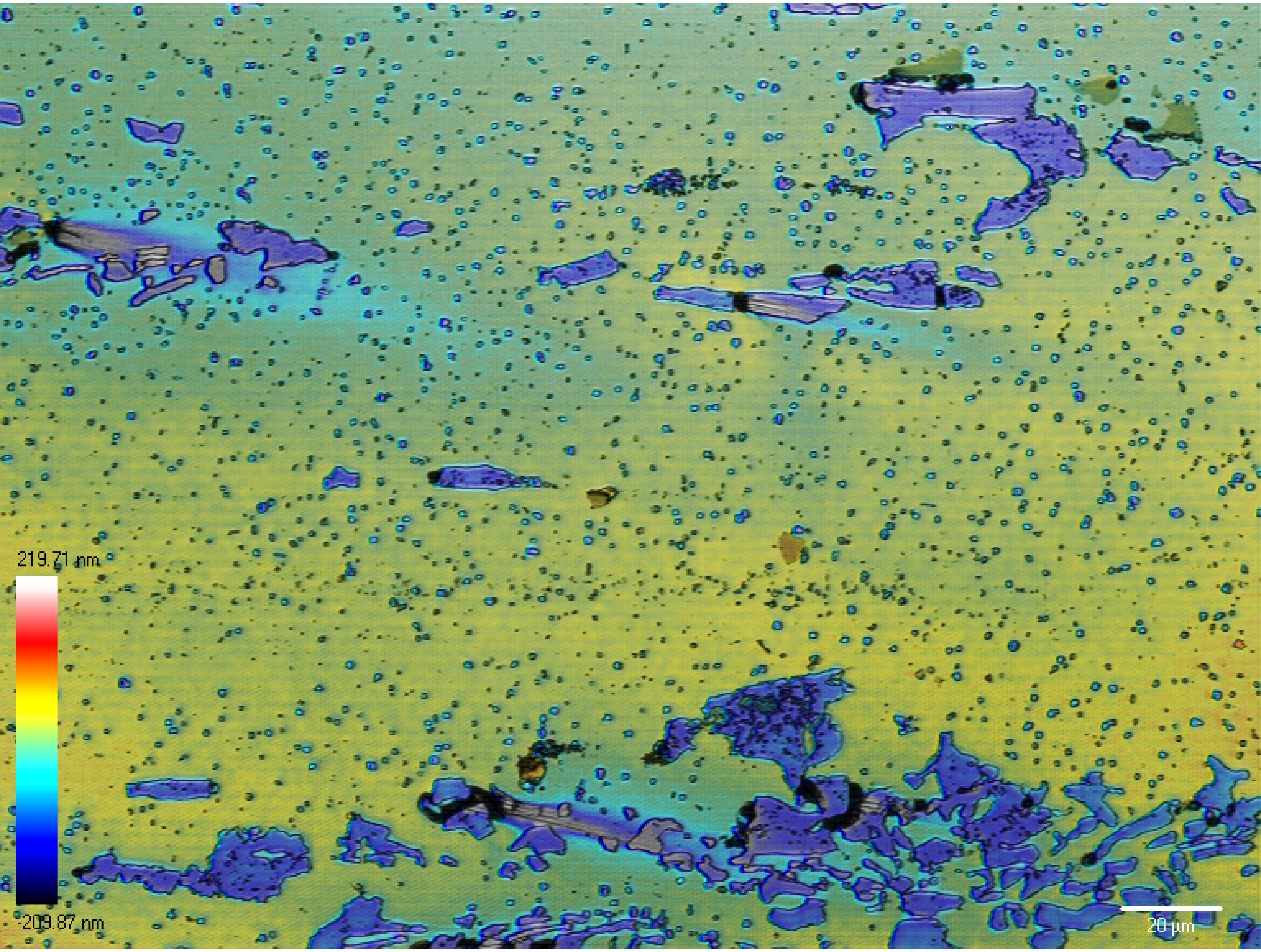
219.71 nm
-209.87 nm
20 µm

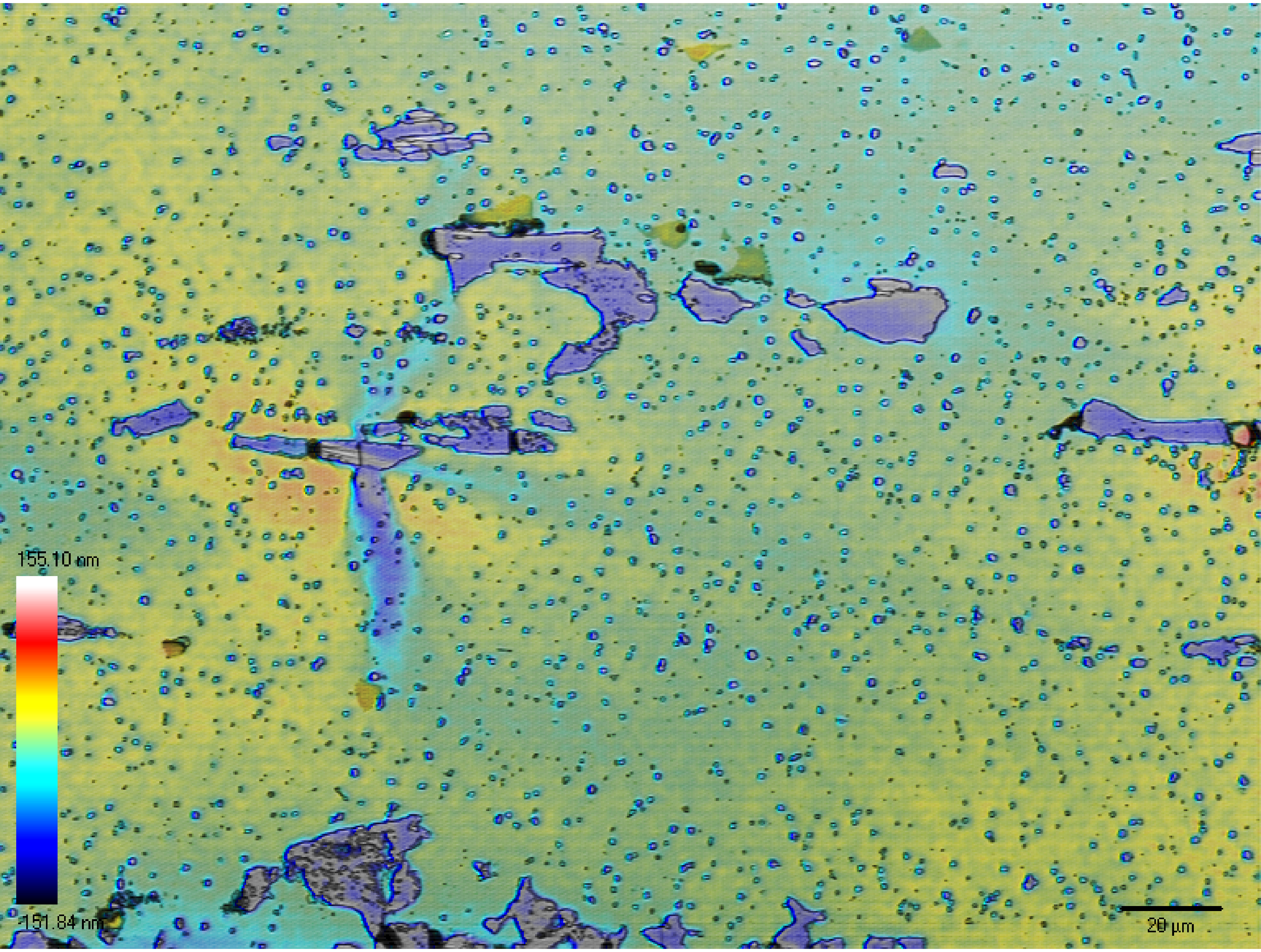
155.10 nm
-151.84 nm
20 µm

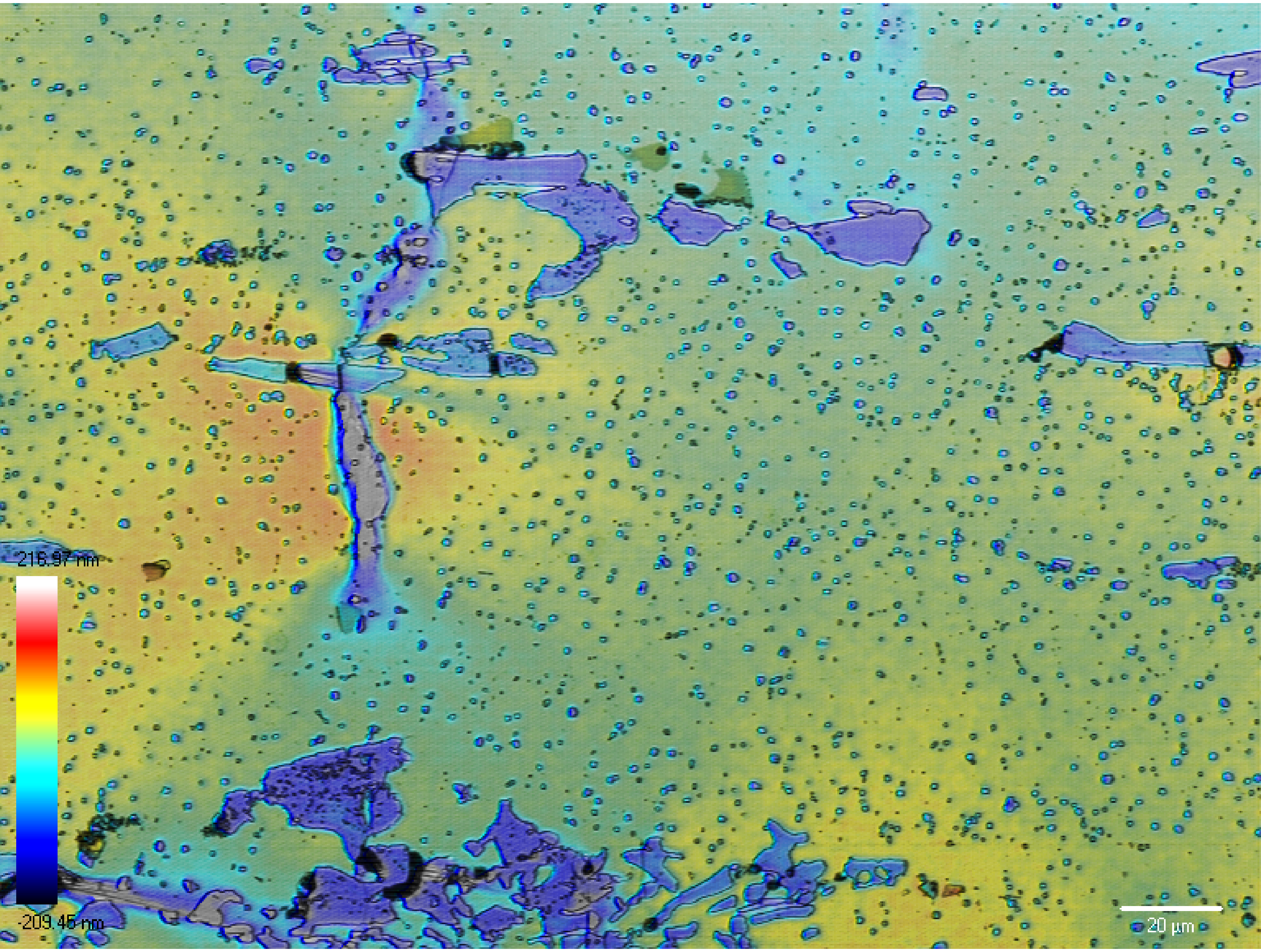
216.97 nm
-209.45 nm
20 µm

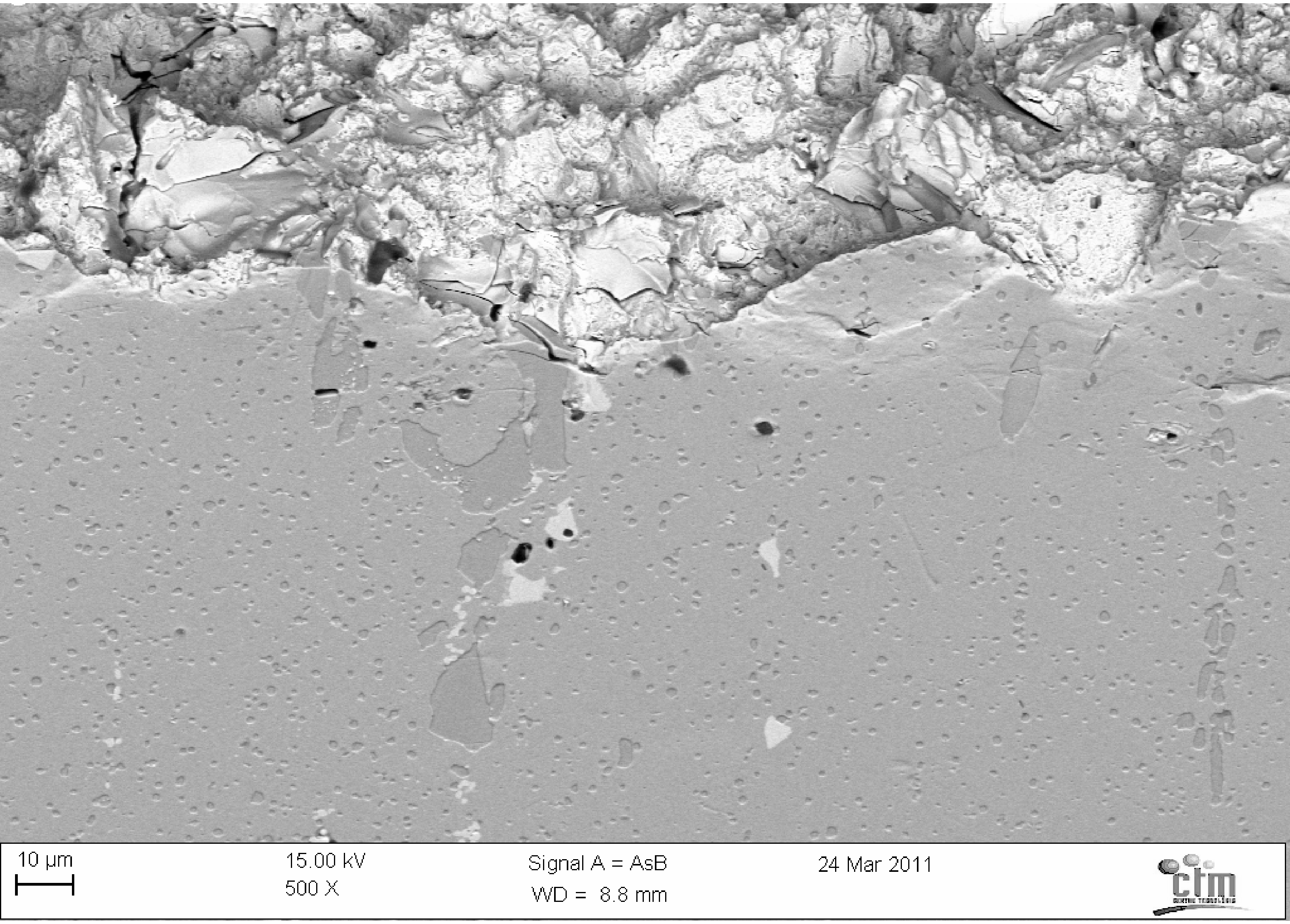
10 µm
15.00 kV
500 X
Signal A = AsB
WD = 8.8 mm
24 Mar 2011
ctm

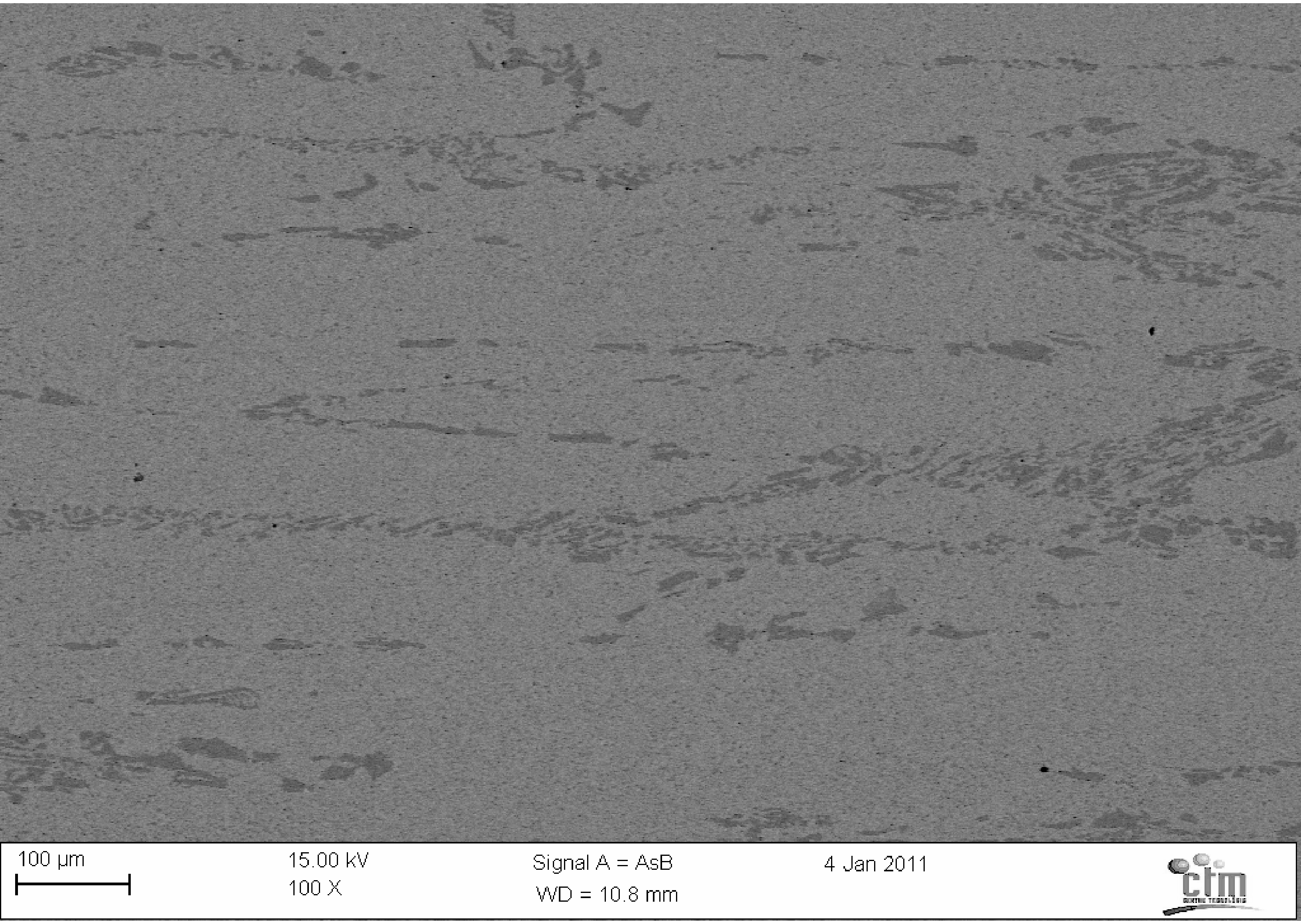
100 µm
15.00 kV
100 X
Signal A = AsB
WD = 10.8 mm
4 Jan 2011
ctm

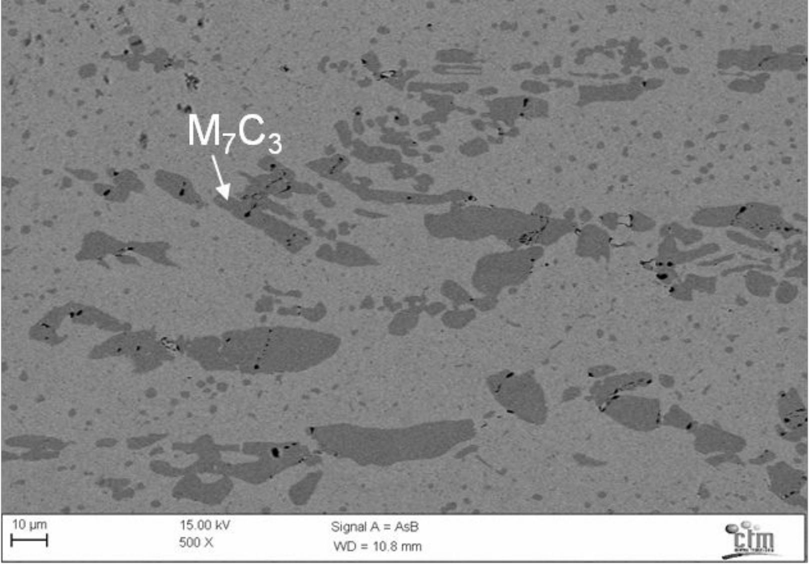
M7C3
10 µm
15.00 kV
500 X
Signal A = AsB
WD = 10.8 mm
ctm

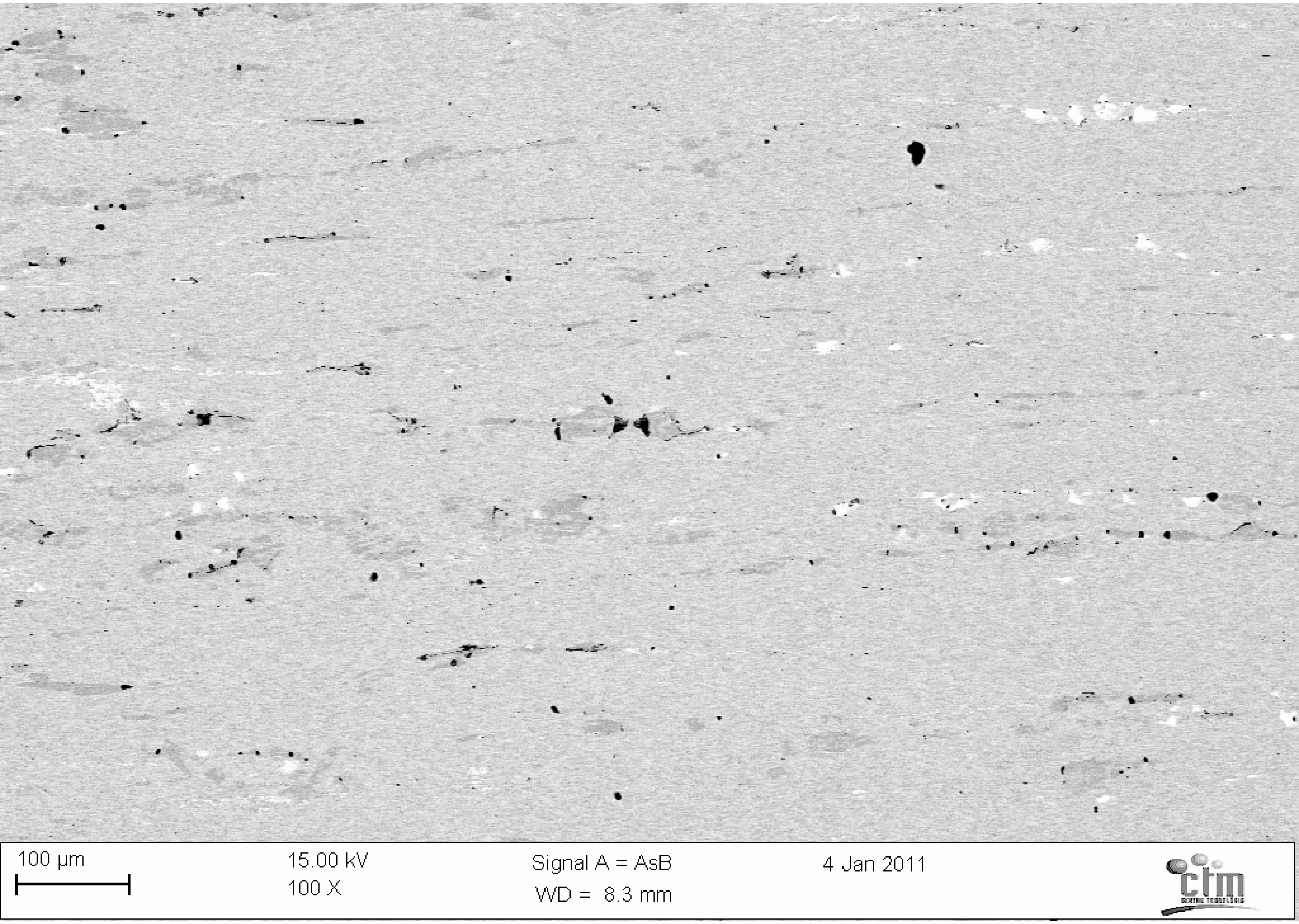
100 µm
15.00 kV
100 X
Signal A = AsB
WD = 8.3 mm
4 Jan 2011

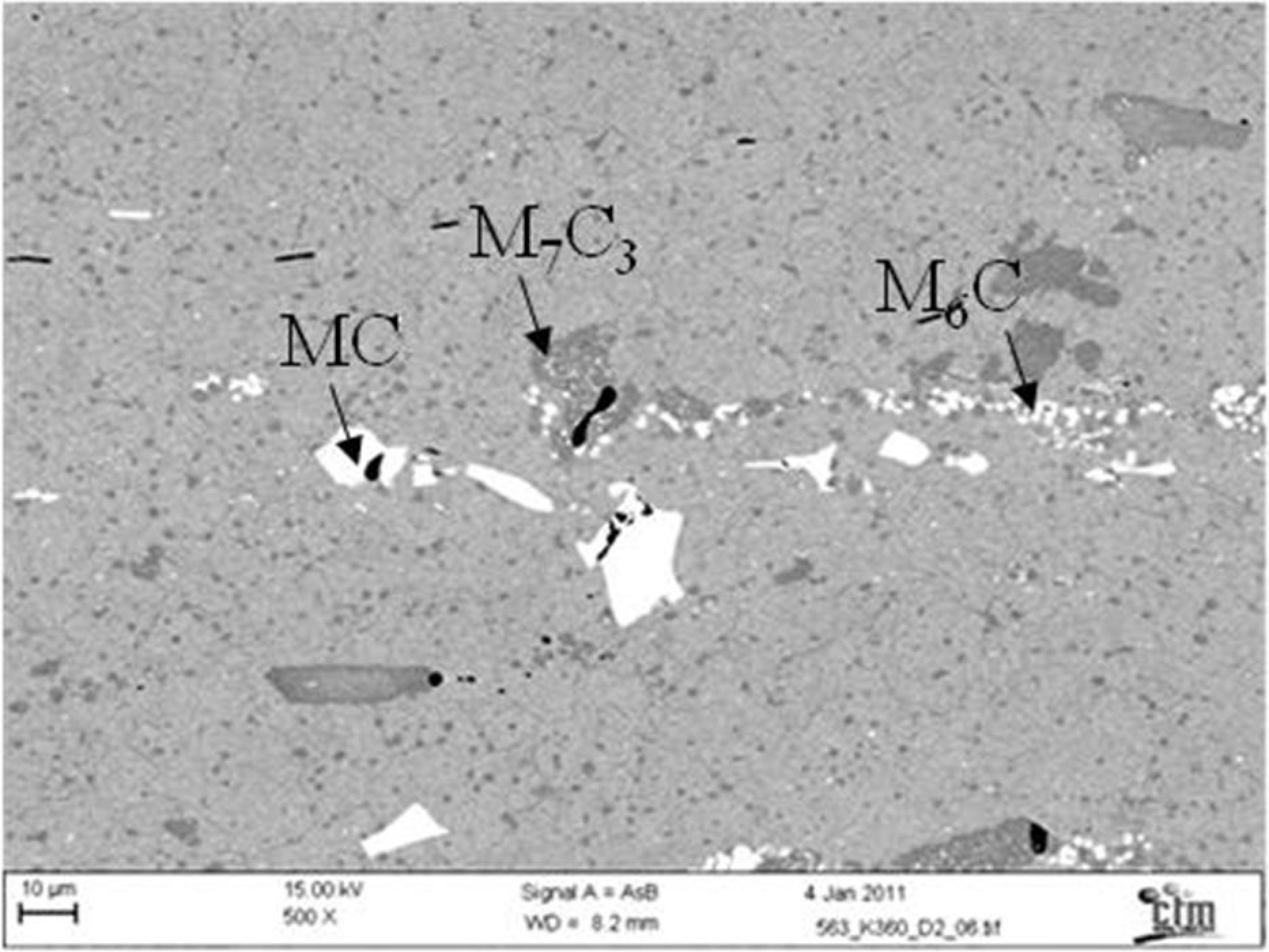
M$_7$C$_3$
M$_6$C
MC
10 µm
15.00 kV
500 X
Signal A = AsB
WD = 8.2 mm
4 Jan 2011
563_K360_D2_06.tif

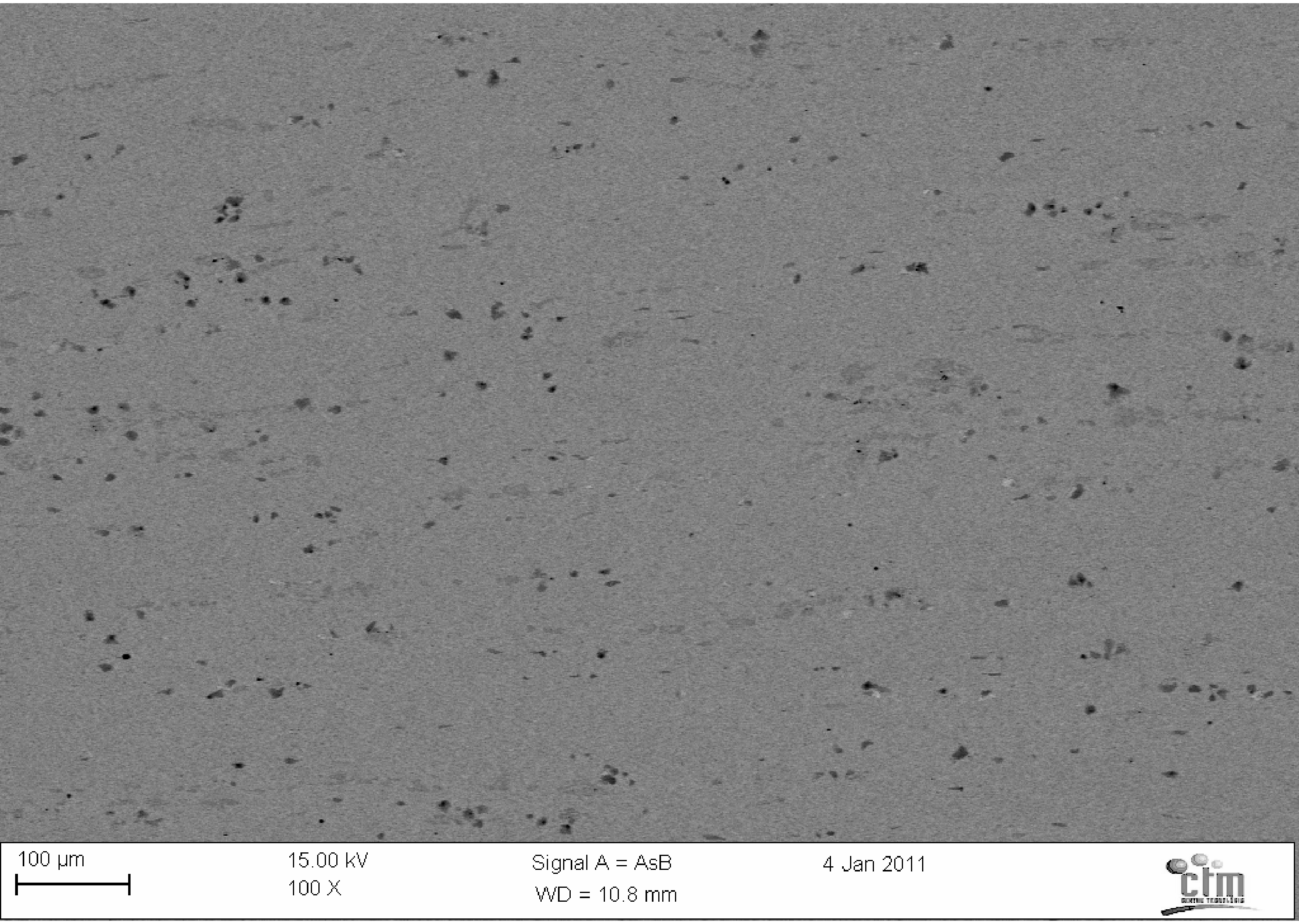
100 µm
15.00 kV
100 X
Signal A = AsB
WD = 10.8 mm
4 Jan 2011
ctm

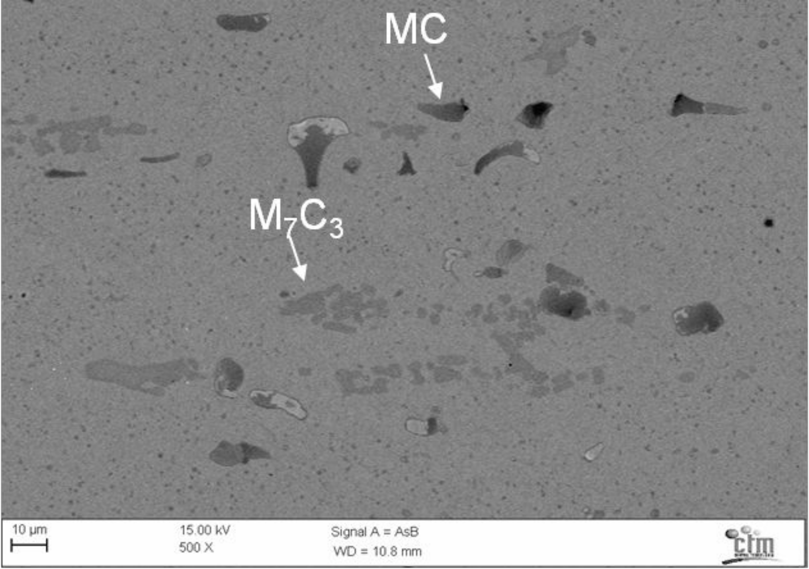
MC
M_7C_3
10 µm
15.00 kV
500 X
Signal A = AsB
WD = 10.8 mm
ctm

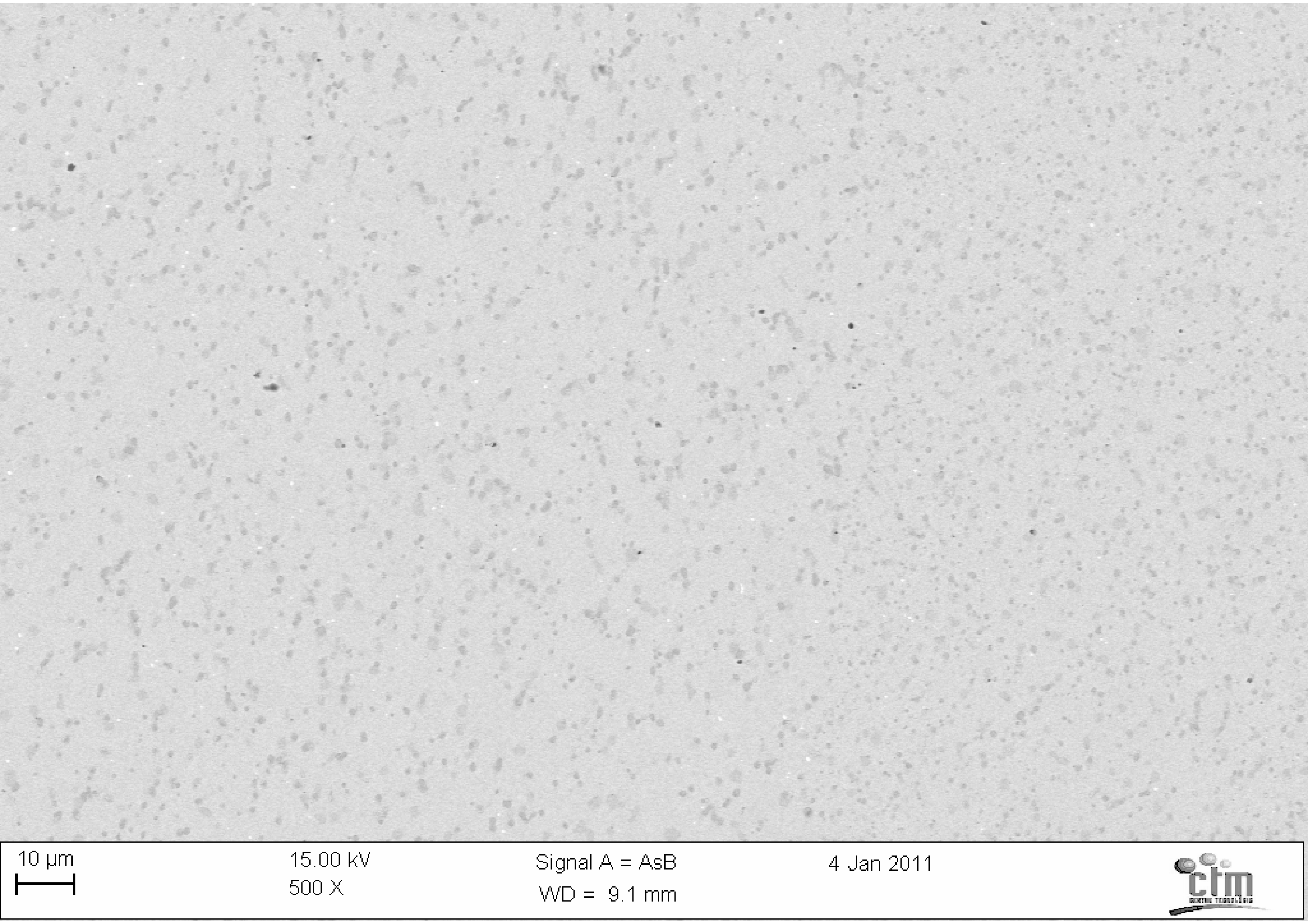
10 µm
15.00 kV
500 X
Signal A = AsB
WD = 9.1 mm
4 Jan 2011
ctm

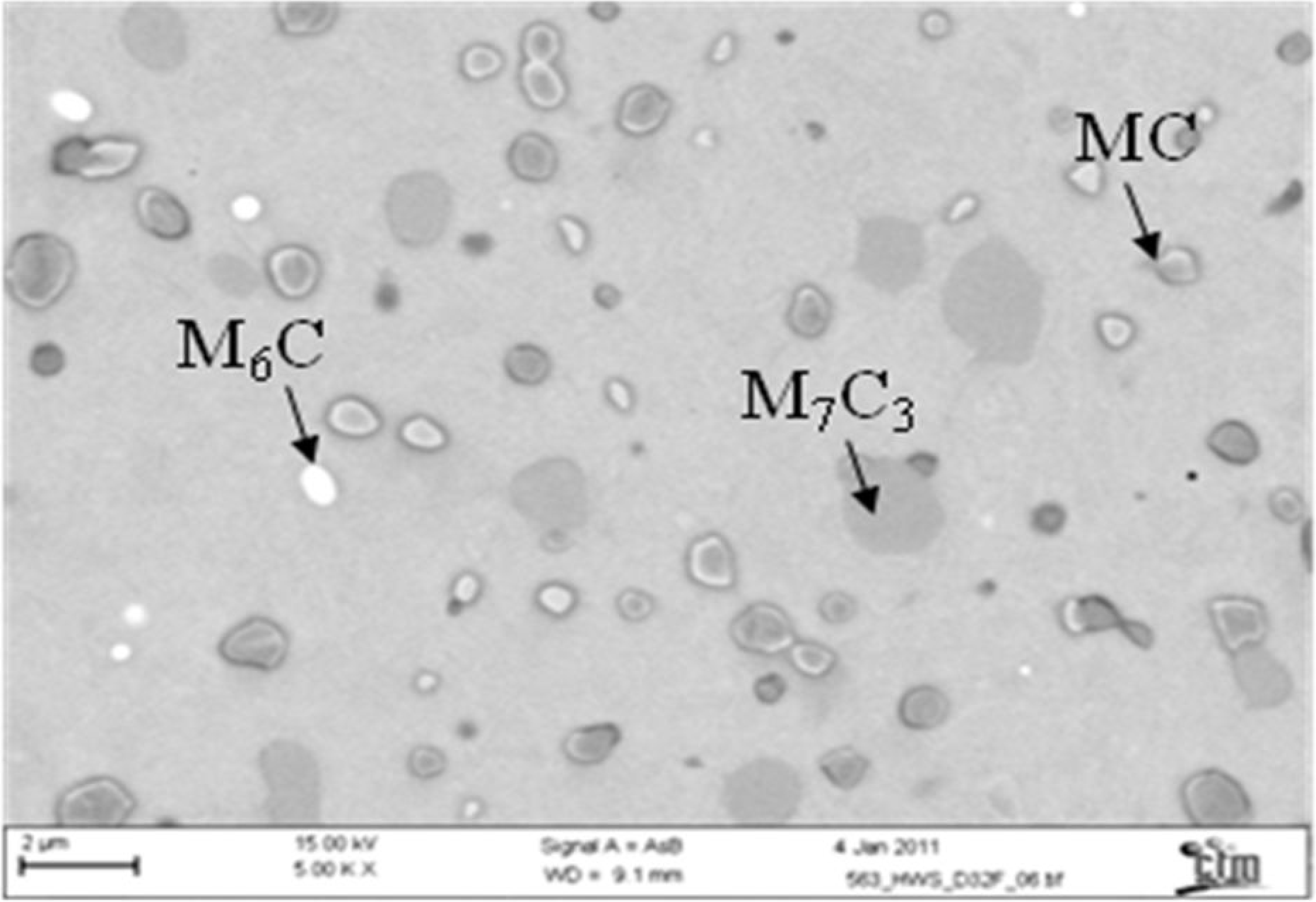
MC
M$_6$C
M$_7$C$_3$
2 µm
15.00 kV
5.00 K X
Signal A = AsB
WD = 9.1 mm
4 Jan 2011
563_HWS_D03F_06.tif

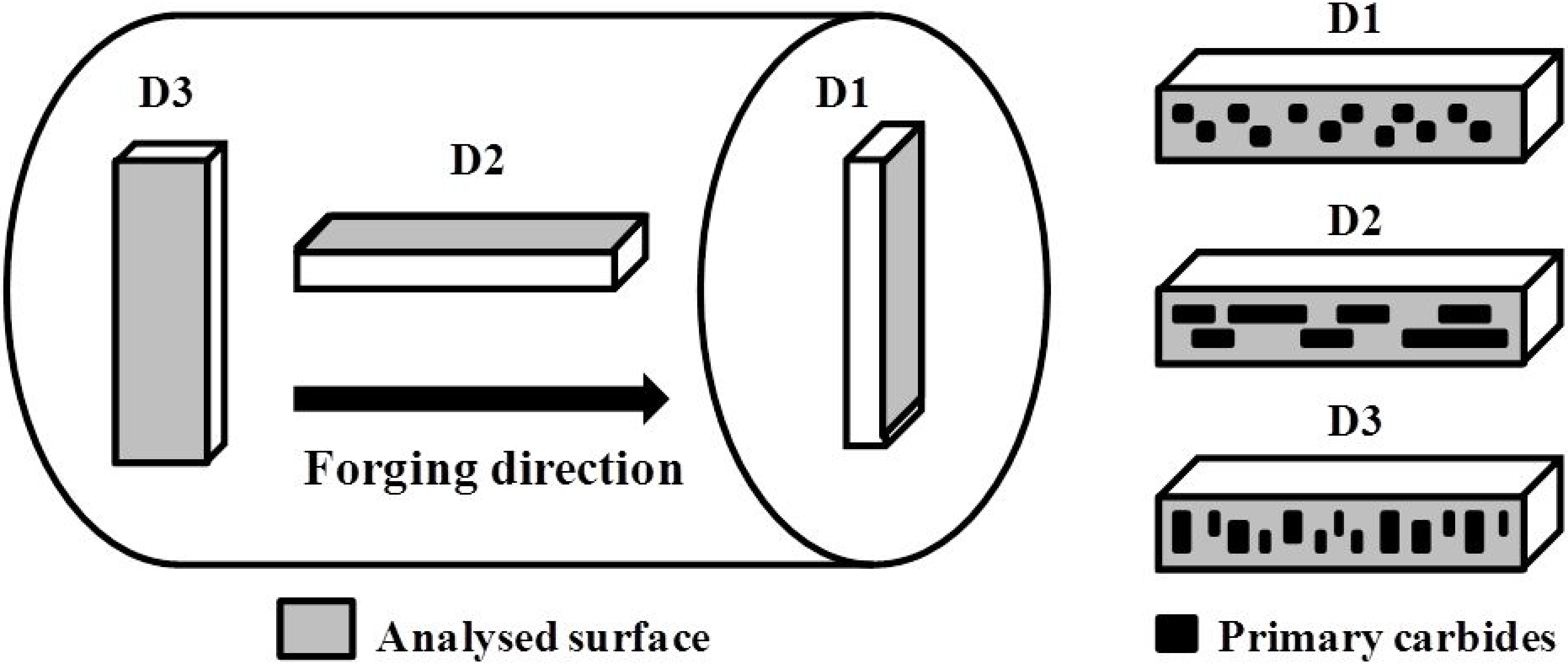
D3
D2
D1
Forging direction
Analysed surface
D1
D2
D3
Primary carbides

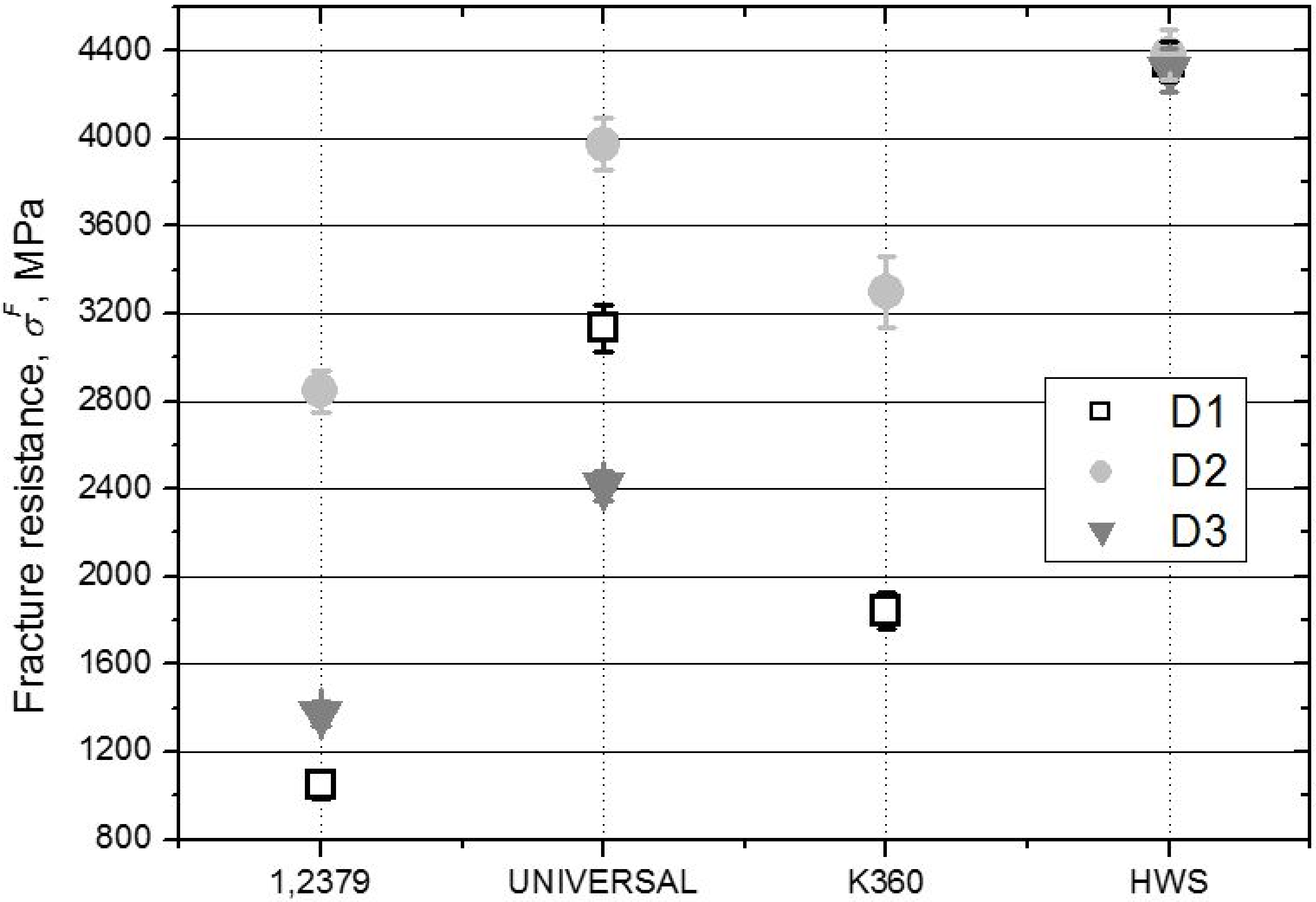
Fracture resistance, σ^F, MPa
4400
4000
3600
3200
2800
2400
2000
1600
1200
800
1,2379
UNIVERSAL
K360
HWS
D1
D2
D3

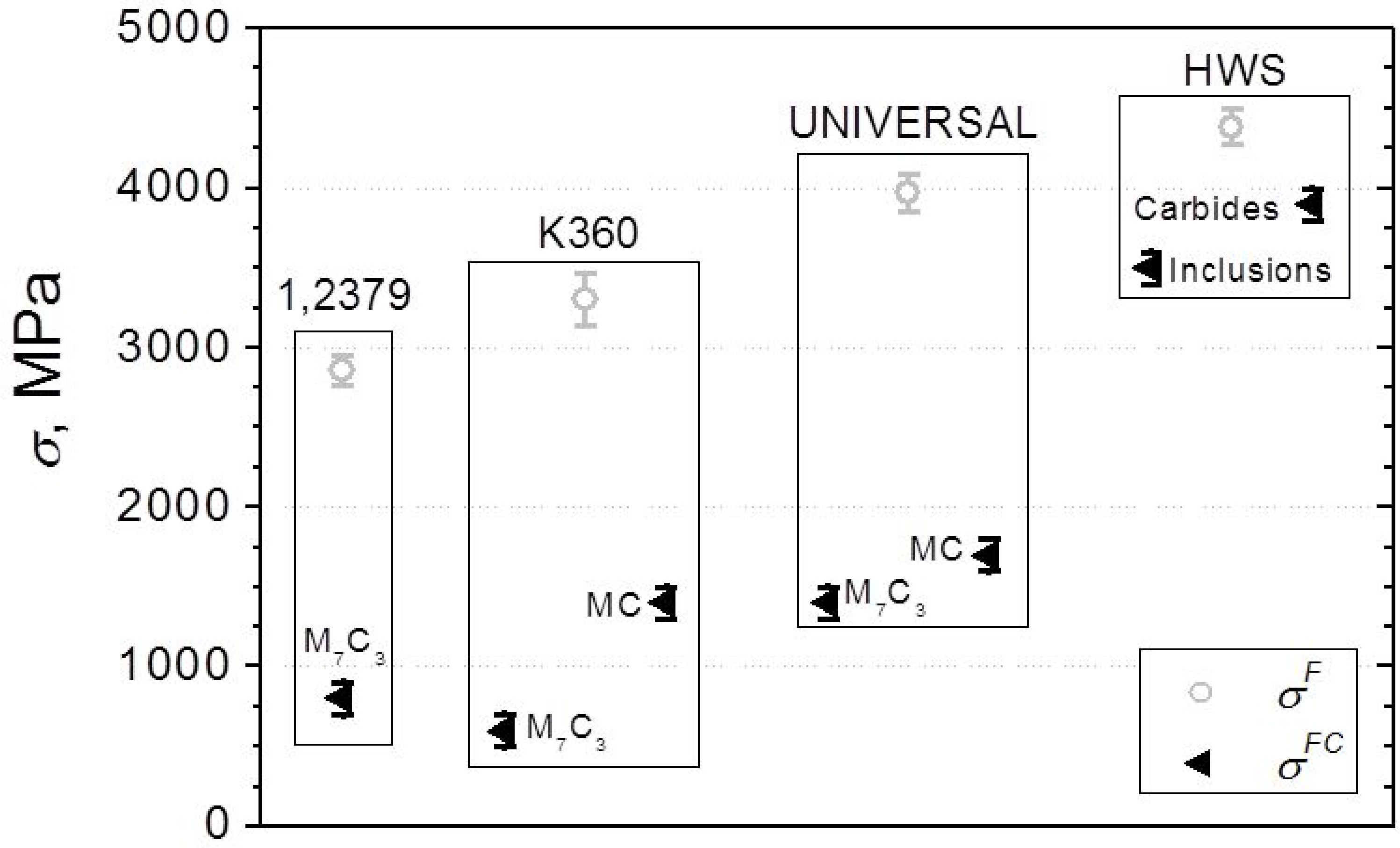
σ, MPa
0
1000
2000
3000
4000
5000
1,2379
M_7C_3
K360
MC
M_7C_3
UNIVERSAL
MC
M_7C_3
HWS
Carbides
Inclusions
σ^F
σ^{FC}

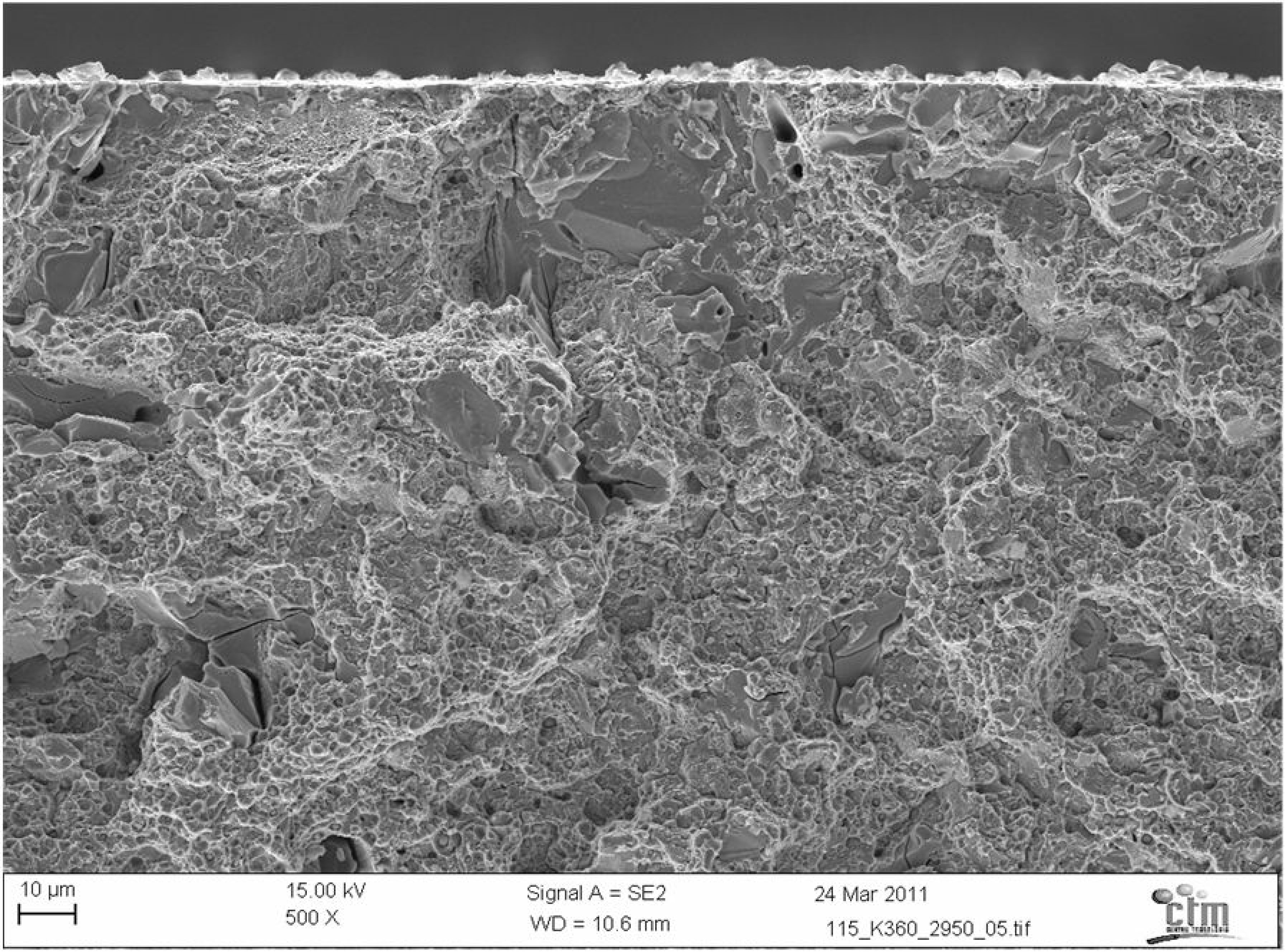
10 µm
15.00 kV
500 X
Signal A = SE2
WD = 10.6 mm
24 Mar 2011
115_K360_2950_05.tif

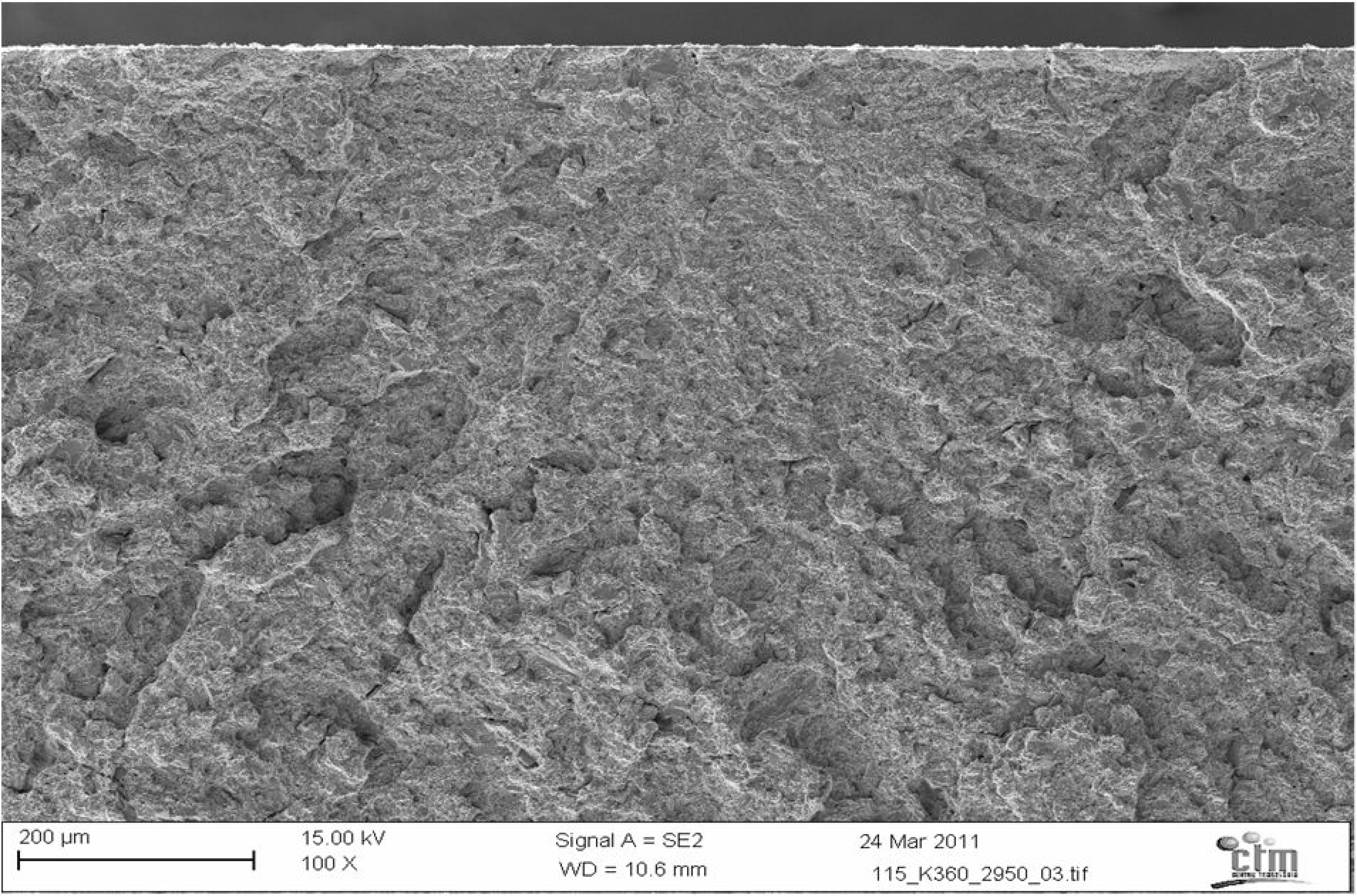
200 µm
15.00 kV
100 X
Signal A = SE2
WD = 10.6 mm
24 Mar 2011
115_K360_2950_03.tif
ctm

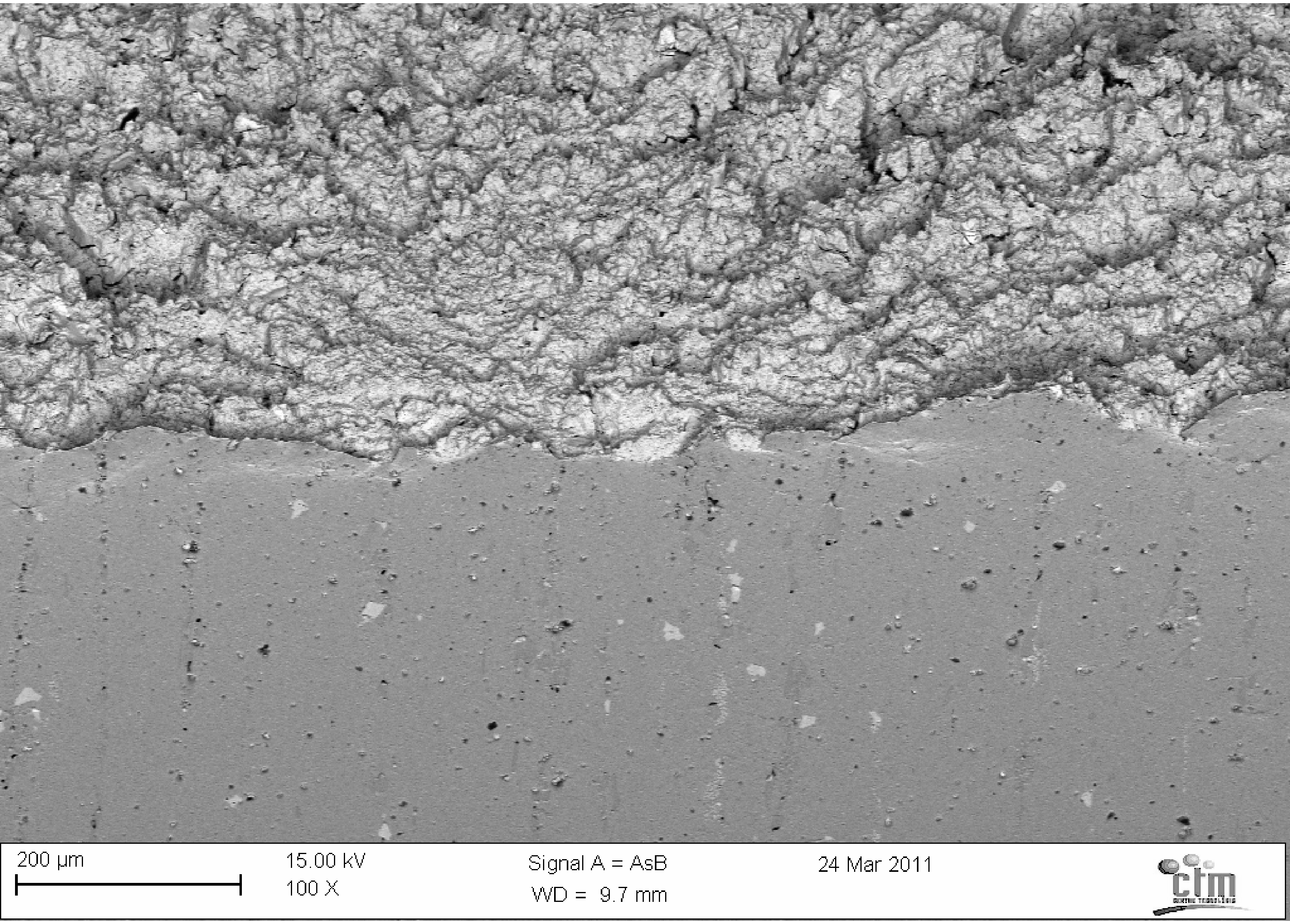
200 µm
15.00 kV
100 X
Signal A = AsB
WD = 9.7 mm
24 Mar 2011
ctm

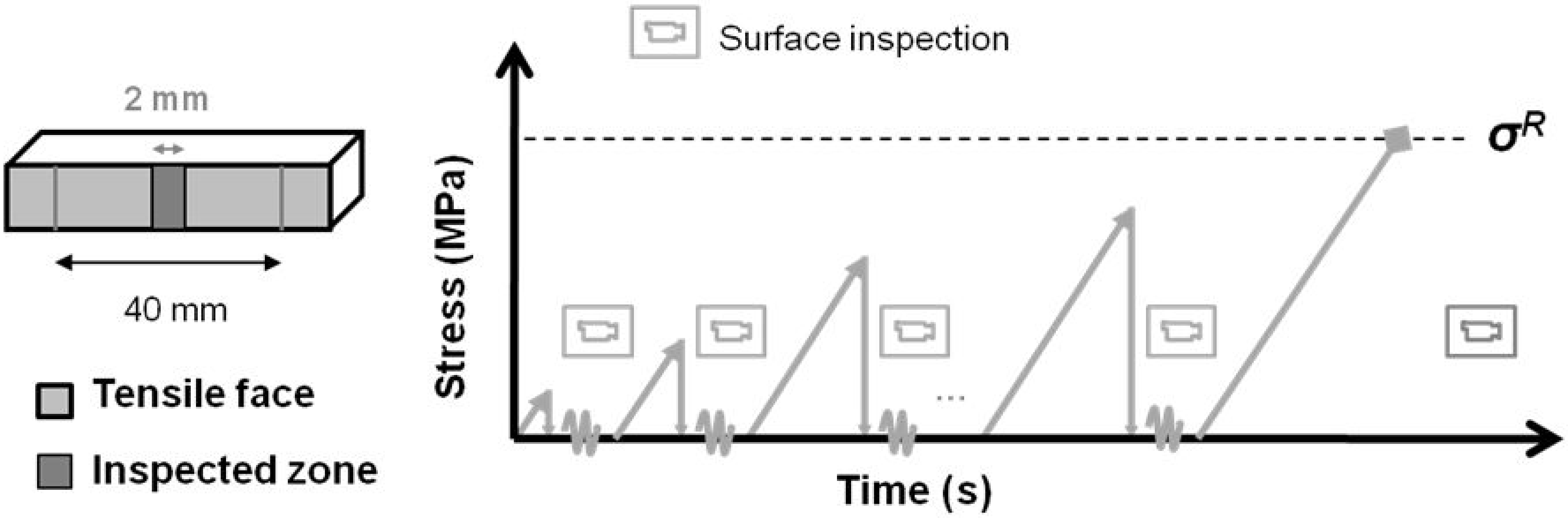2 mm
40 mm
Tensile face
Inspected zone
Surface inspection
σ^R
Stress (MPa)
Time (s)
...